PSFC/JA-05-23

Evidence for electromagnetic fluid drift turbulence controlling the edge plasma state in the Alcator C-Mod tokamak

B. LaBombard, J.W. Hughes, D. Mossessian, M. Greenwald, B. Lipschultz, J.L. Terry,
and the Alcator C-Mod Team

September 2005

Plasma Science and Fusion Center
Massachusetts Institute of Technology
Cambridge MA 02139 USA

This work was supported by the U.S. Department of Energy, Grant No. DE-FC02-99ER54512.

Evidence for electromagnetic fluid drift turbulence controlling the edge plasma state in the Alcator C-Mod tokamak

B. LaBombard*, J.W. Hughes, D. Mossessian, M. Greenwald, B. Lipschultz, J.L. Terry, and the Alcator C-Mod Team

Massachusetts Institute of Technology, Plasma Science and Fusion Center
175 Albany St., Cambridge, MA 02139 USA

Plasma profiles across the separatrix and scrape-off layer (SOL) in Alcator C-Mod are examined for a range of plasma densities, currents and magnetic fields in ohmic L-mode discharges and for a subset of conditions in ohmic H-mode discharges. In all plasmas, electron pressure gradient scale lengths (L_{pe}) exhibit a minimum value just outside the separatrix (i.e., in the *near* SOL), forming the base of a weak (strong) pedestal in L-mode (H-mode) plasmas. Over a wide range of conditions in ohmic L-mode discharges, L_{pe} at this location are found to track with a monotonic function of electron collision frequency, when this quantity is normalized according to the framework of electromagnetic fluid drift turbulence theory. Moreover, at fixed values of normalized collisionality (characterized as the 'diamagnetic parameter', α_d), electron pressure gradients in the near SOL increase with plasma current squared, holding the MHD ballooning parameter, α_{MHD}, unchanged. Thus, the state of the near SOL is restricted to a narrow region within this two-parameter phase-space. An implication is that cross-field heat and particle transport are strong functions of these parameters. Indeed, as α_d is decreased below ~0.3, cross-field heat convection increases sharply and competes with parallel heat conduction along open field lines, making high plasma density regions of α_{MHD}-α_d space energetically inaccessible. These observations are consistent with the idea that the operational space of the edge plasma, including boundaries associated with the tokamak density limit, are controlled by electromagnetic fluid drift turbulence.

PACS: 52.25.Fi, 52.25.Gj, 52.35.Ra, 52.55.Fa

* Tel.: 1-617-253-7264, Fax: 1-617-253-0627: e-mail: labombard@psfc.mit.edu

1. Introduction

The edge plasma region, a zone that extends across the last closed flux surface into the scrape-off layer, plays a key role in the performance of a tokamak fusion reactor. For H-mode plasmas, the height of the 'pedestal' formed in this region directly affects the overall energy confinement properties of the discharge [1-4]. In high density discharges, cross-field heat convection in this zone can precipitate divertor detachment and may be an essential ingredient in the empirically observed density limit scaling law [5]. In all discharges, the particle and heat load distributions in the divertor and onto first-wall components depend on transport in this region. These mechanisms ultimately set the impurity concentrations in the discharge and determine the effectiveness of the divertor in compressing gases and controlling neutral pressures in the main-chamber.

Despite the importance of the edge plasma to reactor operation, reliable physics-based prescriptions for the cross-field transport fluxes and resultant plasma profiles in this region remain to be assembled. This is because the underlying physics involves a nonlinear, self-consistent coupling between fully-developed plasma turbulence and transport, and the equilibrium plasma profiles in the presence of neutral transport and plasma fueling – a complex system that can not yet be simulated from first-principles numerical computation. Nevertheless, significant progress towards this goal has been made in recent years on two fronts: (1) Detailed experimental observations of plasma profiles, fluctuations, and turbulence in the edge of existing experimental devices have allowed a more complete picture of these phenomena to be assembled and (2) theoretical descriptions of edge plasma transport has progressed, primarily through the development of computational tools to simulate plasma turbulence in a 3-D tokamak geometry.

A leading theoretical framework for edge plasma turbulence and transport can be broadly classified as low-frequency electromagnetic fluid drift turbulence [6, 7]. Because the edge plasma tends to reside in a collision-dominated regime, a fluid description is often justified. Consequently, a number of 3-D turbulence simulation codes [8-10] have been built on a set of Braginskii-like plasma fluid equations [11], coupled with an electromagnetic model that accounts for finite inductance in parallel Ohm's law and handles the associated magnetic field perturbations. This research has identified key parameters that control the character and magnitude of the turbulence and cross–field transport in simulated 'edge plasmas'. Among these are the local plasma pressure gradient normalized to the poloidal magnetic pressure (~α_{MHD}, the MHD ballooning parameter) and a normalized plasma collisionality (e.g. parameter C_0 in [8] or the diamagnetic parameter, α_d, in [9]). An additional geometrical complexity in this system is the transition from closed to open magnetic field lines. However, in a collisional fluid-like regime, which is required for the models' validity, the boundary condition at the ends of field lines is not expected to play a dominant role. Therefore, for a fixed magnetic topology, the same 'control parameters' are expected to govern the transport dynamics in regions near the last-closed flux surface. The turbulence code, BOUT [12], explicitly models the separatrix and open field line regions. It has been used to explore their influences, including an effect of enhanced electrical resistivity arising from magnetic shear near x-point regions [13]. A 'resistive x-point mode' is observed that enhances cross-field transport near the x-point and on the low-field region of the SOL [14].

Cross-field particle and heat transport diffusivities are typically deduced from the time-averaged, flux-gradient relationships that are observed in the turbulence simulations. These have

been compiled for different control parameter values, mapping out the 'phase-space' of electromagnetic fluid drift turbulence.

In light of the detailed experimental measurements of plasma profiles, fluctuations, and transport that now exists in tokamaks, some key questions may be addressed: To what extent do the 3-D turbulence simulations capture the experimentally observed plasma response? Does the underlying theoretical framework of electromagnetic fluid drift turbulence (EMFDT) contain the essential physics? For example, do the 'control parameters' as identified in numerical simulations play the expected role in actual experiments? These questions serve as the primary motivation for the experimental investigation described in this paper. However, our research approach is a bit different than one might initially expect: Rather than attempt to measure time-dependent plasma fluctuation dynamics with sufficient accuracy and detail, we focus our attention instead on the 'edge plasma state', i.e. the time-averaged densities, temperatures, gradients and cross-field fluxes, at a well-diagnosed location in the edge plasma of Alcator C-Mod where EMFDT is expected to play a dominant role.

We begin our investigation in section 2 with a review of the transport phenomenology observed in the scrape-off layers of tokamaks. This discussion sets the stage for a subsequent focus on the plasma conditions just outside the last-closed flux surface (i.e. in the *near* scrape-off layer). It is argued that if a time-averaged, flux-gradient relationship is to exist somewhere locally in the edge plasma, then it ought to be observed at this location. An overview of the experimental setup, covering key diagnostics and discharge conditions used to assemble data for the present investigation, is compiled in section 3.

Cross-field plasma profile data from scanning Langmuir probe and Thomson scattering diagnostics are presented in section 4. Data from a wide range of ohmic L-mode discharges and a

small set of ohmic H-mode discharges are included. The quality of the data are critically assessed and some general trends are noted. In all discharges, a minimum in electron pressure gradient scale length is seen just outside the separatrix. Unlike at other locations in the SOL, normalized ion saturation current and floating potential fluctuations are found to be relatively low at this location, with fluctuation statistics tending to exhibit near-Gaussian probability distribution functions.

Section 5 covers the heart of our experimental investigation. Here we look for connections between the observed plasma state in the near scrape-off layer and local control parameters as identified in EMFDT. For this purpose, the experimentally observed edge plasma conditions are mapped onto the phase-space of EMFDT. Clear connections with EMFDT theory are indeed found in the L-mode data set: pressure gradient scale lengths are found to track remarkably well as a monotonic function of plasma collisionality, when normalized according to EMFDT. In addition, for fixed values of this parameter, normalized electron pressure gradients ($\sim\alpha_{MHD}$) are found to remain unchanged in discharges with different plasma currents and toroidal magnetic fields. In contrast, H-mode data points are seen to 'break through' this apparent limit on poloidal beta-gradient, attaining up to ~50% higher α_{MHD} values locally. Thus, it appears that the turbulence-suppression mechanism associated with the H-mode can also extend into the near SOL.

The remaining content of section 5 focuses on cross-field fluxes and their relationship to normalized collisionality (C_0 [8] or α_d [9]). Here we make use of a previously developed technique to estimate cross-field fluxes directly from experimental data [15]. Effective cross-field particle diffusion (D_{eff}) and convection (V_{eff}) coefficients are compiled and the role of

cross-field heat convection on SOL power balance is revisited. Again, collisionality, as defined by EMFDT, is found to behave as an excellent 'control parameter', yielding similar values of D_{eff} and V_{eff} over a range of plasma currents and magnetic fields. These new experimental results clearly supersede previous ones – studies where D_{eff} and V_{eff} were correlated against a crude power law function of electron-ion mean free path normalized to parallel connection length [5] or a function of discharge density normalized to the density limit [16]. Nevertheless, all these pseudo-control quantities are intimately related. Indeed, our experimental observations support the hypothesis that the tokamak 'density limit' is fundamentally a *transport limit*, relating to an operational boundary in the phase space of EMFDT that can not be crossed, owing to an explosive growth of cross-field transport fluxes. Section 6 makes broader connections between the present results and observations on other tokamaks. Section 7 enumerates and summarizes the principal research findings.

2. Background: scrape-off layer transport phenomenology

Over the past few years a new understanding of transport phenomena in the edge and scrape-off layer (SOL) regions has emerged [17], both from detailed analysis of edge fluctuation phenomena (e.g. [5, 18-25]) and from direct visualization of edge plasma turbulence with imaging systems (e.g. [26-28]). Plasma appears to intermittently 'peel away' in clumps from the *near* SOL, a zone of steep density and temperature gradients just outside the separatrix, and to propagate quasi-ballistically in the *far* SOL towards main-chamber wall surfaces. These 'transport events' in the far SOL are captured as large amplitude 'bursts' in time-series data from probes and visible diodes (see Fig.1) and as field-aligned filaments or 'blobs' in camera-imaging data. Fluctuation time series data exhibit highly skewed probability distribution functions (PDFs)

with an overall dynamical behavior that is reminiscent of a self-organized critical system [29, 30] (e.g., a 'sand pile'), exhibiting avalanche-like transport phenomena. While the true underlying plasma dynamics are not yet resolved, the behavior hints of two principal ingredients: (1) a threshold condition, such as exceeding a critical gradient, which leads to the formation of plasma clumps and (2) a mechanism for rapid cross-field transport of the clumps. Since the time-averaged density profiles in the far SOL are relatively flat, these observations point to the near SOL as regulating the transport fluxes via some critical-gradient condition.

A similar blob-like transport phenomenology is found in both L and H-mode confinement regimes. However in H-mode plasmas, the transport events during inter-ELM periods carry smaller fluxes than in L-mode plasmas. Instead, steady-state H-modes achieve a comparable level of time-averaged particle flux by throwing out very large plasma clumps during ELM events. Such ELM-induced blobs also propagate in the far SOL, appearing as large-amplitude versions of the blobs seen in L-mode plasmas [31, 32]. In some H-mode regimes, ELMs are of low amplitude and high frequency (e.g. 'grassy' ELMs) and/or are replaced by a quasi-coherent edge mode (e.g., the EDA H-mode on Alcator C-Mod [33, 34]). Thus, regardless of plasma regime, a time-averaged stationary state is maintained by intermittent (or quasi-coherent) transport across the boundary plasma; the amplitudes and frequencies of the 'transport events' are inversely related, as required in order satisfy steady-state particle and energy balance.

Once the plasma is broken into field-aligned clumps, the mechanism for its radial propagation in the far SOL is readily understood: curvature drift causes a dipole-like polarization of the clumps, resulting in a rapid $E \times B$ convection outward in major radius (e.g. [30, 35]). This physics accounts for the large outward plasma convection velocities and tendencies for flattened time-averaged density and temperature profiles that are observed in the far SOL. It should be

noted that the same physics can explain the radial propagation of the largest plasma clumps – those spawned by type-I ELMs [32, 36] – which can be seen to strike wall components (e.g. JET [37]). Under conditions when the neutral density in the far SOL is sufficiently high, the plasma density in the clumps can be sustained by ionization, which competes against particle losses along open field lines [38]. The result can be a large, time-averaged particle flux to main-chamber wall surfaces, resulting in a 'main-chamber recycling' phenomena, as observed in Alcator C-Mod [15, 39].

The bursty, blob-like transport phenomena is observed to exist primarily (perhaps only) on the low-field side of the torus, a behavior that is also consistent with a curvature-drive model for the far SOL transport. Recent experiments with double-null discharges on Alcator C-Mod have also revealed a reduced level of cross-field transport fluxes on the high-field side of the torus, even in the near SOL [40]. The observed ballooning-like cross-field transport asymmetry appears to drive strong plasma flow along field lines in the SOL. At present, it is unclear if such strong flows play a self-regulatory role in affecting the turbulence and cross-field fluxes (e.g. via changes in toroidal velocity shear profiles).

In contrast to the far SOL, the near SOL normally exhibits little evidence of large amplitude, intermittent, transport phenomena (see Fig.1); the PDFs in this zone tend to be near-Gaussian; gradients in density and temperature are steep. (An exception to this is during an ELM event, which we do not consider here.) Therefore, one might presume the transport fluxes in this zone to adhere to a diffusive-like, flux-gradient paradigm. Indeed, earlier transport scaling analyses had success in correlating local values of D_{eff} to local collisionality [5]. Yet, no such relationship was found to make sense in the far SOL where the time-averaged density profile could be flat – a purely convective transport model, such as blob polarization and $E \times B$

convection, is clearly required. Hence, in comparison to the far SOL, the near SOL looks like a 'transport barrier'; steep gradients are required there to drive the self-consistent cross-field particle and energy fluxes. In L-mode discharges, this 'barrier' region is weak. While in H-mode discharges, the near SOL forms the base of the 'pedestal' that extends further onto closed flux surfaces. Therefore, for a desired set of plasma conditions just inside the separatrix, the near SOL region appears to be responsible for setting the associated level of cross-field transport fluxes, which propagate through the remainder of the SOL.

In light of these observations, our attention is focused squarely on conditions in the near SOL and the time-averaged flux-gradient relationships that may exist there. Most importantly, this is a region where EMFDT is thought to be an appropriate description of the plasma transport dynamics. In this paper, we adopt a simple and straightforward experimental approach: map out the phase space of the near SOL in Alcator C-Mod under a variety of plasma currents, fields and densities, and compare it with that expected from EMFDT.

3. Experimental arrangement

A cross-section of Alcator C-Mod [41] is shown in Fig. 2, indicating the locations of pertinent edge plasma diagnostics. All data reported in this paper were obtained during the run campaigns of 2000 and 2001 using a lower x-point magnetic equilibrium (as shown in Fig. 2) with toroidal field (B_T) and plasma current (I_p) aligned and $B \times \nabla B$ pointing down. High resolution plasma density and electron temperature profiles were recorded by edge Thomson scattering [42] and horizontal-scanning Langmuir probe [43] systems.

A vertical-scanning Langmuir/Mach probe was also employed, primarily to record the poloidal projection of plasmas flows ($E \times B$ plus parallel flow) toward the outer divertor leg.

The measurements of plasma density, temperature and flows, combined with midplane Ly_α brightnesses [44] are used to compute local ionization profiles and to perform a simple particle balance analysis. In this way, the particle flux across the separatrix and SOL regions is estimated and tracked systematically as plasma parameters are changed. Figure 2 shows the location of the toroidally-viewing Ly_α chords. Details of the particle balance analysis technique can be found in [15], which makes use of the 'main-chamber recycling' regime that is typically present in Alcator C-Mod.

The horizontal scanning probe was also used to record basic information on plasma fluctuation levels. The RMS deviation of local ion saturation currents (I_{sat}) and floating potentials (V_f) about their mean values (frequency bandwidth of 5-500 kHz) were recorded during the probe's transit across the SOL.

The two probes were scanned across the SOL two or three times during a single discharge. Simultaneously acquired probe and Thomson data are mapped onto poloidal flux surfaces, reconstructed from magnetic measurements [45] and the EFIT plasma equilibrium code [46]. The flux-surface coordinate that is used in this paper, ρ, is defined as the distance into the SOL along a major radius at the outer midplane. In some low-to-moderate density discharge cases, small shifts in the ρ-axis (up to 2 mm) have been applied to probe or Thomson-inferred profiles, using SOL power balance as a constraint. The impact of flux-surface mapping uncertainties on the conclusions drawn in this paper is discussed in section 4.

Data were collected from both ohmic L-mode and ohmic H-mode plasmas. (Note: Auxiliary RF heating systems were not employed here. This enabled the scanning probes to sample plasma at or just inside the separatrix and to avoid possible RF-sheath rectification effects that can lead to ambiguities in data interpretation.) Ohmic L-mode plasmas were

produced with five different combinations of plasma current, I_p, and toroidal magnetic field, B_T, yielded three different values of safety factor at the 95% flux surface, q_{95} = ~3.5, ~5 and ~6.5. Figure 3 illustrates the parameter space that was covered: a factor of 2 variation in I_p and a factor of 1.5 variation in B_T. Line-averaged density ($\overline{n}_e$) scans were performed at each of the nominal combinations of (I_p, B_T), with a range of variation up to $0.15 < \overline{n}_e / n_G < 0.5$, where n_G is the empirical discharge density limit [47].

A smaller set of ohmic H-modes were also investigated. As indicated in Fig. 3, these were obtained when q_{95} was reduced below about ~3.5. The data traces in Fig.4 show the recipe that was followed to produce both ELM-free and EDA H-mode phases in ohmic discharges. In two of the discharges studied here, scanning probe profiles were obtained in consecutive L and H-mode phases.

4. Plasma profile data

In principle, the edge Thomson and horizontal scanning probe data can be combined to construct composite edge plasma profiles, extending from ~2 cm inside the separatrix to the shadow of the main-chamber limiter structures. However, since our goal is to look for variations in the edge plasma state as external controls (I_p, B_T, $\overline{n}_e$) are varied, it is important that we first assess the level of confidence in these data – Are systematic trends detected by these diagnostics a reflection of the true variation in plasma conditions, or are they influenced in some way by experimental deficiencies/artifacts? To address this question, we first compare edge plasma profiles obtained separately from each diagnostic, focusing on overlapping regions where both diagnostics are expected to report reliable data. Then, we construct composite profiles that span

the entire edge region. This exercise serves to document the cross-field profiles that are observed in ohmic L and H-mode regimes (both ELM-free and EDA) on Alcator C-Mod.

4.1. Density and temperature

Electron density (n), temperature (T_e) and pressure ($p_e = nT_e$) profiles from the edge Thomson and horizontal scanning probe systems are shown in Fig. 5. These representative profiles were taken from ohmic L-mode discharges with $I_p = 0.8$ MA, $B_T = 5.4$ T and for a set of line-averaged densities, $\bar{n}_e = 1.1, 1.3, 1.4, 1.9 \times 10^{20}$ m^{-3}. Each curve shown is a smooth spline fit to ~15 Thomson points (~1.3 mm radial resolution, blue curves) and ~200 probe points (obtained during inward and outward probe scans, two electrodes, ~0.5 mm resolution, red curves). It should be noted that for locations inside the separatrix ($\rho < 0$) the scanning probe tends to underestimate the electron temperature and to overestimate the plasma density relative to the Thomson system. The effect may be due to an over-heating of the probe and/or related to a high level of plasma recycling on the probe surface, a phenomenon that has been directly observed by monitoring the dispersion of impurities injected by the vertical probe [48]. In any case, these probe data are treated with suspicion and are not used for quantitative analysis. For regions at or outside the separatrix ($\rho > 0$), the T_e values obtained from both diagnostics are found to overlay reasonable well. However, the probe systematically records a higher density, suggesting that the ion collection areas may be underestimated. As $\bar{n}_e$ is changed, both diagnostics see a trend of flattening nT_e profiles near the separatrix ($\rho = 0$). Thus, the pressure profile shapes appear to be accurate, even if the absolute density levels may be offset by a multiplicative factor.

In ohmic H-mode discharges (Fig. 6), the profiles have much sharper gradients near the separatrix. The pressure profiles from both diagnostics overlay reasonable well, lending further confidence to the inferred nT_e gradients, even as the pressure profiles become very steep.

The differences between ohmic L-mode and H-mode profiles are explored further in Fig. 7. The color-coded curves represent averages of several profiles from similar discharges. Composite profiles for each discharge are first generated; data (d_i) at a specific location (ρ_i) is computed as a weighted sum of probe (d_i^p) and Thomson (d_i^T) data according to the rule: $d_i = fd_i^p + (1-f)d_i^T$, with $f = 1$ for $\rho_i \geq 2$ mm and $f = exp(\rho_i / 2 - 1)$ otherwise. The ELM-free and EDA H-mode profiles shown in Fig. 7 correspond to discharges in Fig. 3 with $0.7 < I_p < 0.8$ MA. Profiles are also shown for a series of similar ohmic L-mode discharges ($I_p = 0.8$ MA, $B_T = 5.3$ T), binned into four different line-averaged density categories.

H-mode profiles show the characteristic 'pedestal' in T_e and n, which extends partially across the last-closed flux surface into the near SOL. The density in the far SOL is noticeably higher in EDA versus ELM-free H-modes, consistent with a higher level of time-averaged plasma recycling that is associated with EDA. Yet, L-mode discharges also exhibit a weak pedestal structure that spans into the near SOL region.

L-mode profiles are remarkably sensitive to plasma density. As the density is raised, pressure gradient scale lengths near the separatrix become systematically longer; the far SOL develops a broad density shoulder; electron temperatures there rise slightly at first. These observations are suggestive of an increasing level of cross-field heat and particle transport, with a convective component in the far SOL. For discharges with densities at or exceeding a level of $\bar{n}_e / n_G \sim 0.5$, the weak pedestal structure associated with the separatrix disappears; electron

temperatures *inside* the separatrix drop substantially. Thus, cross-field transport (i.e. flux-gradient proportionalities) appears to be an ever increasing function of density in these discharges, consistent with the idea that transport physics plays a fundamental role in the empirically observed tokamak density limit [5, 49].

4.2. Fluctuations

Fluctuation data from the horizontal scanning probe are assembled in Fig. 8. These data are taken from a set of discharges similar to those represented in Fig. 7. The quantities shown are the RMS deviations about the mean values of local ion saturation currents (I_{sat}) and floating potentials (V_f) over a frequency bandwidth of 5-500 kHz.

Apart from the highest density case with $\overline{n}_e / n_G \sim 0.5$, normalized I_{sat} and V_f fluctuations tend to increase with distance from the separatrix. In general, discharges with the strongest pedestal-like features in Fig. 7 (H-modes, low density L-modes) exhibit the lowest fluctuation levels (both normalized and absolute) in the near SOL. In L-mode discharges, an overall trend of increasing fluctuation level with plasma density is seen. However, normalized I_{sat} and V_f fluctuations remain at or below ~20% in the near SOL for all but the highest density case. Everywhere in the SOL, EDA H-modes exhibit higher absolute fluctuation levels compared to ELM-free, consistent with the relatively higher level of plasma flux/recycling that is observed; the increase in normalized I_{sat} fluctuations seen near the separatrix in EDA (relative to ELM-free) is caused by a ~100kHz quasi-coherent mode [33, 34, 50-52].

The fluctuation data shown here merely augment the more extensive set of turbulence observations made in a number of other tokamaks (see review in section 2). However, all these data are consistent with the notion that transport across the entire SOL is determined largely by

the transport properties in the vicinity of the separatrix – the effect of the quasi-coherent fluctuation in EDA H-modes is a clear example (albeit, a special case). However, as we focus our attention on the near SOL, we need to be mindful of regimes where the large-amplitude, intermittent transport of the far SOL invades the near SOL, rendering a simple time-averaged flux-gradient transport model to be invalid. Such a situation is indeed found as the discharge density limit is approached [16]. The data in Figs. 7 and 8 for L-mode discharges with $\bar{n}_e / n_G \sim$ 0.5 already show the beginnings of this trend: profiles inside the separatrix are flattened and normalized fluctuations levels in the near SOL are similar to those of the far SOL.

4.3. Pressure gradient scale lengths in the *near* SOL

From the profiles in Fig. 7, we see that, in all cases, the local electron pressure gradient scale length, $L_{Pe} \equiv \left| \partial ln(nT_e) / d\rho \right|^{-1}$, exhibits a minimum just outside the separatrix. The value depends on plasma conditions, e.g., confinement regime, L-mode plasma density. Figure 9 examines this trend in more detail, comparing estimates of L_{pe} derived separately from probe and Thomson data. Within the scatter of the measurements, both computations of L_{pe} yield similar values in the near SOL, tracking with the changing plasma conditions. Not surprisingly, the scanning probe data exhibit less scatter; the probe is expected to operate most reliably in this region. Moreover, L_{pe} is a convenient parameter since it insensitive to systematic density calibration errors (i.e., a multiplicative factor) that may exist in the processed data.

It is important to note that for all profiles, L_{pe} exhibits a minimum near the location ρ = 2 mm. This feature in the profile acts as a 'marker' and tells us that our magnetic flux surface mapping is reproducible to within a discharge-to-discharge accuracy of about ±1 mm. The

absolute accuracy of the ρ-mapping with respect to the true separatrix location is estimated to have a similar uncertainty range. While one may be tempted to 're-adjust' the ρ-mapping such that the minimum in L_{pe} occurs at $\rho = 0$, we find that such an adjustment would lead to an inconsistency – heat conduction into the divertor would not match the heat into the SOL. (This test is performed in low-to-moderate density discharges where the contribution of cross-field heat convection to the SOL power balance is low.)

In the remainder of this paper, we focus our attention on the plasma conditions measured by the horizontal scanning probe at the location where the minima in L_{pe} tend to occur, i.e., at $\rho = 2$ mm. This location is particularly convenient for a number of reasons: (1) it defines an unambiguous location in the profile, independent of flux surface mapping concerns; (2) it is in the near SOL zone, a location where EMFDT should apply, and (3) it is a location where reliable, high spatial resolution probe data is obtained.

5. Phase space of the near scrape-off layer

5.1. Electromagnetic fluid drift turbulence – control parameters

Direct numerical simulation of electromagnetic fluid drift turbulence in the plasma edge have been performed by a number of researchers. In particular, Scott [8, 53] and Rogers, Drake, Zeiler, *et al.* (RDZ [9, 54-56]) have independently identified a set of key dimensionless parameters that govern the plasma dynamics and control the character and magnitude of the turbulence and resultant cross-field transport. The system of equations studied by these two groups is very similar – a set of Braginskii fluid equations, augmented to account for electromagnetic effects, including magnetic induction in parallel Ohm's law and field line distortion via associated poloidal magnetic field fluctuations. The only principle difference in the

two approaches is the way the state variables are normalized. Scott uses a 'drift-wave scaling' while RDZ normalize according to a linear resistive-ballooning paradigm (see Table 1 for a subset of the definitions used). Scott has also extended the range of validity into more collisionless regimes by including finite electron inertia and an additional equation to evolve the parallel electron heat flux with a Landau damping term [8]. Nevertheless, both lines of investigations have found that the saturated state of the plasma turbulence and transport has little to do with linear instability mechanisms; non-linear coupling mechanisms rule, with a competition between primary turbulence drive and the growth of secondary instabilities that regulate the overall turbulence/transport levels. Therefore, among other things, these studies have highlighted an important fact: It is not possible to assemble transport scaling relationships based only on linear instability models; these relationships are largely irrelevant for predicting the saturated state of the turbulence and resulting transport. Instead, one must be resigned to map out the phase-space of the turbulence and transport, as defined by the dimensionless parameters that control the plasma dynamics.

Through a number of studies with increasing increments of sophistication, Scott [8, 53] and RDZ [9, 54, 55] have identified the most important control parameters for EMFDT. These are: (1) local plasma pressure gradient normalized to the poloidal magnetic pressure (i.e., poloidal beta gradient) and (2) the electron-ion plasma collision frequency normalized to characteristic turbulence time-scales (collisionality). Owing to the use of different normalizations, these parameters take on different forms in the two systems (see Table 1). However, for fixed background gradients, the parameters α_{MHD} and α_d (RDZ) are strictly proportional to $\hat{\beta}$ and $C_0^{-1/2}$ (Scott). Magnetic shear ($\hat{s} = r\left(\partial q / \partial r\right)/q$, in these cylindrical

models) is also found to be an important parameter [6, 8], but it is not a significant variable in the fixed magnetic topologies that we are investigating here.

The turbulence simulations were performed within the context of a 'local approximation', i.e., with background plasma profiles characterized by 'gradient parameters' (as listed in Table 1). Implicit in this approach is the assumption that the turbulent fluctuation levels are small compared to background values (another reason that our focus is on plasma turbulence in the near SOL region as opposed to the far). In addition, the background profiles are not self-consistently 'relaxed' during the simulations, regardless of the magnitude of the resultant cross-field transport levels, which can approach remarkably high diffusion coefficients, ~100 m^2/s. Nevertheless, these numerical investigations provide a rough guide to the landscape of turbulence and transport phenomena in the phase-space of EMFDT.

Heat and particle diffusivities are found to be strong, non-linear functions of both beta gradient (α_{MHD} or $\hat{\beta}$) and collisionality (α_d or C_0) in some regimes. For example, a regime of very large cross-field transport at high collisionality and low beta gradient was identified by RDZ [9]. This regime was associated with the onset of a transport-defined tokamak density limit (see Fig. 10). In addition, due to electromagnetic effects in these models, cross-field transport was found to increase strongly with beta gradient, well before the onset of the ideal MHD limit ($\alpha_{MHD} \sim 1$) [8, 54]. RDZ also noted a change in character of the turbulence at large α_d (low collisionality), leading to a regime where transport could *decrease* with increasing α_{MHD}. It was speculated that such a bifurcation of the flux-gradient relationships might lead to a region of α_{MHD}-α_d space where L to H-mode transitions would spontaneously occur [9]. This threshold condition has been developed further by Guzdar *et al.* [57] and has been found to make contact with observations of edge pedestal gradients in DIII-D [58] and C-Mod [59].

Recently, Xu and coworkers [14, 60] have used the BOUT code to study EMFDT as the tokamak density limit is approach. As in other simulations, the turbulence is evolved on top of specified 'background' plasma profiles. However, BOUT incorporates the full 3D magnetic geometry (including the x-point) and the turbulence is modeled across the entire SOL. The simulations were found to qualitatively reproduce the 'density-limit' behavior as originally identified by RDZ: a rapid increase in cross-field transport was recorded as density was raised (α_d decreased) or plasma current reduced (α_{MHD} increased). However, the simulations did not appear to cross a 'density-limit boundary' when the toroidal field was changed (or equivalently, safety factor, q, was changed). As plasma density was increased towards the empirical limit, a transition from a resistive x-point mode to a resistive ballooning mode was observed. It was speculated that the x-point mode might be responsible for removing the q-scaling that is implicit in RDZ's density-limit boundary.

5.2. Phase space accessible to real plasmas

In contrast to the numerical simulations described above, the gradients in real plasmas are not externally controlled but are constrained to satisfy particle and power balance. Over a characteristic transport time scale, the profiles adjust themselves; outward particle fluxes must match neutral fueling rates and outward energy fluxes must match heating power. How then does the measured plasma state relate to the phase-space identified by EMFDT simulations? One may expect only portions of the space to be accessible to real experiments; the portion beyond a 'density-limit boundary' would be excluded, for example. Similarly, regions with low transport levels might also be inaccessible; on a transport timescale, the plasma would steepen its gradients (e.g., α_{MHD} or $\hat{\beta}$) and 'climb out' of these zones. In principle, the latter behavior may

be partly compensated by lowing the input power and/or gas fueling rate. However, these changes also affect the plasma collisionality (e.g., α_d or C_0), pushing the system to a different phase-space location.

If cross-field transport is a sensitive function of location in the two-parameter phase space, α_{MHD}-α_d or equivalently $\hat{\beta}$-C_0, as suggested by numerical simulations, then the locus of accessible stationary states in a real experiment might effectively collapse onto one (or more) characteristic curve(s) in this space. For example, the plasma's normalized beta gradient might appear as a single-parameter function of the plasma's normalized collisionality. Thus, a simple experimental test is suggested: vary the externally-controlled machine parameters (I_p, B_T, $\overline{n}_e$) over a wide range. If the resultant edge plasma states are found to cluster around characteristic curves in the dimensionless phase space that defines EMFDT, then it is likely that EMFDT physics is indeed controlling the flux-gradient relationships.

With these ideas in mind, we now proceed to examine the plasma states that are observed in the near SOL of Alcator C-Mod.

5.3. Ohmic L-mode discharges

5.3.1 Gradient scale lengths in the Near SOL

We begin by looking for functional relationships between electron pressure gradient scale lengths (L_{pe}) and normalized collisionality. Figure 11 shows measurements of L_{pe} from ohmic L-mode discharges at the location ρ = 2 mm, plotted versus the square-root of electron-ion mean-free-path, λ_{ei}, normalized in three different ways: (a) by major radius, $\left(\lambda_{ei}/R\right)^{1/2}$, (b) by parallel connection length, $\left(\lambda_{ei}/qR\right)^{1/2}$, and (c) by q times magnetic connection length

$\left(\lambda_{ei}/q^2R\right)^{1/2}$. The latter dimensionless quantity is of interest because it explicitly appears in the EMFDT parameters, α_d and C_0 (see Table 1). The parallel connection length normalization, (b), leads to another parameter of interest for SOL phenomena; the transition from sheath-limited to conduction-limited parallel heat transport regimes depends on λ_{ei}/qR, for example. Finally, the major-radius normalization, (a), yields a collisionality parameter that is independent of q.

The data shown in Fig. 11 were obtained from L-mode discharges that had a factor of 2 variation in I_p and a factor of 1.5 variation in B_T (see Fig. 3). Points are color-coded according to the safety factor at the 95% flux surface, q_{95}, which is used in the normalizations ($q = q_{95}$). Of the three collisionality parameters, the last one does the best job of compressing the L_{pe} measurements into a one-parameter relationship. The q-dependences in the other normalizations are too weak. These data are very suggestive; the EMFDT parameters, α_d or C_0, appear to contain the relevant collisionality normalization – one that can be used to express the local gradients in terms of a quasi-functional dependence over a wide range of plasma conditions.

This tendency is explored further in Fig. 12. Here, density gradient scale lengths, L_n, in addition to L_{pe} are plotted versus α_d and color-coded according to q_{95} and I_p. A remarkably tight grouping of L_n data points about a monotonic function of α_d is observed. The clustering of L_{pe} values is also improved relative to that in Fig. 11. (Although some of the improvement can be ascribed to the $\left(R/L_n\right)^{1/4}$ factor in α_d and the correlation between L_n and L_{pe}.) It should be noted that an alternative plot can also be made that exhibits a similar functional relationship between L_n (or L_{pe}) and Scott's collisionality parameter, C_0.

5.3.2 Beta gradients in the Near SOL

Carrying the analysis forward, we now examine normalized pressure gradients at the location ρ = 2 mm for the same set of discharges. Figure 13 shows measured electron pressure gradients, converted into $\hat{\beta}$ or α_{MHD} and plotted versus the collisionality parameter, α_d. This is a direct mapping of edge plasma states onto the two-parameter phase-space of EMFDT. Again, a remarkable clustering of the data points is observed, exhibiting the following key characteristics:

(1) Despite the wide variation in external parameters (I_p, B_T, $\overline{n}_e$), normalized pressure gradients fall onto a well-defined band in α_{MHD}-α_d (or $\hat{\beta}$-C_0) space, implying a quasi-functional relationship between combinations of α_{MHD} and α_d (or $\hat{\beta}$ and C_0). Apparently, only edge plasma states that are restricted to these combinations are accessible and stable.

(2) The range of the observed α_{MHD} and α_d values is very similar to that considered in EMFDT simulations (see Fig. 10). [However, as noted in section 4.1, the electron densities reported by the probe diagnostic may be systematically high, possibly resulting in overestimated α_{MHD} values (up to ~40%) and underestimated α_d values (~20%).]

(3) As α_d is decreased below ~0.3, normalized pressure gradients (α_{MHD} or $\hat{\beta}$) decrease proportionally. As discussed below in sections 5.5 and 5.6, cross-field transport becomes large in this parameter range, prohibiting the plasma from accessing the region $\alpha_{MHD} >$ ~$3\alpha_d$ for $\alpha_d <$ ~0.3. This behavior is entirely consistent with the location of a 'density limit' boundary, as identified by RDZ (Fig. 10).

(4) Data points from discharges with I_p=0.5 and 1.0 MA are seen to overlay in the parameter

range $0.3 < \alpha_d < 0.4$. Normalized pressure gradients in this range all have $\alpha_{MHD} \sim 0.7 \pm 0.2$, yet they have *absolute* pressure gradients that are different by a factor of ~4 ($\propto I_p^2$).

The latter point is examined in more detail in Fig. 14. Cross-field profiles of absolute and normalized pressure gradients are shown for the discharges in Fig. 13 with α_d near 0.3. Absolute pressure gradients (at ρ = 2 mm) scale roughly as $\propto I_p^2$ [panel (a)], yielding normalized pressure gradients that are indistinguishable, to within the scatter in the data [panel (c)]. In sharp contrast, no explicit dependence on toroidal magnetic field strength is evident [panel (b)]. This behavior suggests the existence of a critical value of α_{MHD}, beyond which the cross-field fluxes grow rapidly.

In summary, the data in Figs. 11-14 form a convincing collection of evidence; EMFDT does indeed appear to control the flux-gradient relationships in the near SOL. Moreover, the clustering of edge plasma states about a fixed beta gradient is indicative of a marginally-stable system, where small changes in gradient lead to large changes in transport fluxes. Such a critical gradient behavior may be precisely what is needed to explain the intermittent, avalanche-like transport phenomena observed in the far SOL, as discussed in section 2.

5.4. Ohmic H-mode discharges

Some additional aspects of the edge plasma's operational phase-space are revealed by comparing the edge states in ohmic H and L-mode phases. L_{pe} and α_{MHD} data from ELM-free and EDA ohmic H-modes are overlaid on top of the L-mode data in Fig. 15, distinguished by symbol and color. These data cover the full range of discharges studied (see Fig. 3). Note that for two discharges, data were collected from both L and H-mode phases; arrows are shown

connecting between these consecutive points.

Most H-mode discharges are seen to 'break through' the apparent L-mode limitations in normalized beta gradient and pressure gradient scale length, approaching a factor of ~2 decrease in L_{pe}. Thus, the near SOL is very much a part of the H-mode pedestal; flux-gradient relationships there are clearly affected. This observation also tells us that the L_{pe} measurements in L-mode are not being limited by diagnostic deficiencies. However, some EDA H-modes have L_{pe} values comparable to L-mode. It should be recalled that EDA measurements were obtained during the ~100kHz quasi-coherent oscillation [33, 34, 50-52], possibly accounting for increased, time-averaged L_{pe} measurements.

L-mode discharges that evolve into H-modes start off at high α_d and subsequently move downwards in α_d as well as upwards in α_{MHD} to their final states (see arrows). The downward α_d trajectory is caused by the H-mode density rise and resultant collisionality increase. [Note that due to power balance constraints on open field lines, the electron temperature is nearly unchanged at this location in the profile (see Fig. 7)]. It is interesting that the H-mode states are found to lie in a restricted α_d range; no data points are found below $\alpha_d \sim 0.27$. Thus, H-modes appear to avoid the high-transport, 'density limit' region of the phase-space, both during their formation and evolution into the final state. This behavior is interesting and implies that only L-mode discharges with sufficiently high α_d can evolve into H-modes. The behavior also consistent with the observation that a minimum value of electron temperature is required just inside the separatix to achieve an L-H transition [61]; plasmas with high cross-field heat transport (low T_e) do not evolve into H-modes. Since $\alpha_d \propto 1/q\sqrt{n}$ at fixed electron temperature, the starting L-mode density and/or q_{95} must not be too high; otherwise, there is no room in α_d-

space for the L-mode to 'grow' into an H-mode. Indeed, our operational experience is consistent with these trends; ohmic H-modes are accessible in C-Mod only when q_{95} is reduced below ~3.5 in moderate to low density plasmas (e.g., Fig. 3).

Finally, the observation that high α_d L-mode discharges are the ones that can evolve into H-mode potentially makes contact with some ideas initially put forward by RDZ [9] and considered further by Guzdar [57]. These studies suggested that there may exist a region in α_{MHD}-α_d space where transport *decreases* with increasing beta gradient. The onset of this stabilization effect is thought to involve a critical beta gradient, $\alpha_{MHD,crit} \approx C / \alpha_d^2$, with the coefficient C being roughly in the range of 0.085–0.12 [57]. It is interesting that the parameterization $\alpha_{MHD} = 0.15 / \alpha_d^2$ (shown as a black dashed line in Fig. 15) does a nice job of marking the boundary of edge plasma states that are observed at high α_d. One could argue that states above this line are rarely observed because they tend to be unstable; they might spontaneously develop into H-modes and move down in α_d. The two arrows shown in Fig. 15 are suggestive of this physics; they run parallel to the dashed line, marking start and near-finish locations of two such transitions into H-mode. (Note that the time-dependent evolution of the edge state, which is not measured here, is likely to trace out a curved trajectory that extends *above* the dashed line.)

In light of these considerations, the recipe used for producing the ohmic H-modes (e.g. Fig. 4) may be understood: the action of ramping down q_{95} serves to move the L-mode state toward increased α_d at fixed α_{MHD}, perhaps crossing a threshold, $\alpha_{MHD,crit}$. After the L-H transition is achieved, q_{95} is ramped back up causing α_d to decrease faster than it would have evolved otherwise, limiting the final value of α_{MHD} in the H-mode phase. This final ramp-up in

q_{95} is found to be an important part of the recipe towards achieving steady EDA H-modes, which tend to exist at higher q_{95} than ELM-free H-modes [1, 33].

5.5. Cross-field particle transport

In earlier work, the scaling of cross-field particle flux densities near the separatrix ($\Gamma_\perp$) with local plasma conditions was examined, revealing a correlation between the effective particle diffusivity, $D_{eff} \equiv -\Gamma_\perp / \nabla_\perp n$, or convection velocity, $V_{eff} \equiv \Gamma_\perp / n$, with local collisionality, $\sim \lambda_{ei} / qR$ [15], and/or line-average density normalized to the density limit, $\bar{n}_e / n_G$ [5, 16]. Here we revisit these relationships, focusing on α_d (and by implication, C_0) as a potentially more appropriate control parameter.

In these studies, $\Gamma_\perp$ values are obtained by solving the particle continuity equation, using measured n, T_e, and Lyα brightness profiles as input. The model, which is described in detail in [5, 15], accounts for particle flows into the divertor and employs measurements of particle fluxes onto main-chamber surfaces. In essence, the technique exploits the tendency for the scrape-off layer fluxes to be dominated by 'main-chamber recycling', causing $\Gamma_\perp$ to be closely related to the ionization source profile in the main chamber (inferred via Lyα emissivity measurements). While the absolute magnitudes of the resulting $\Gamma_\perp$, D_{eff} and V_{eff} are expected to be a factor of ~2 accurate at best, the technique allows such quantities to be tracked systematically as a function of discharge conditions.

Figure 16 shows the result of this procedure applied to the full set of ohmic L-mode discharges. $\Gamma_\perp$, D_{eff} and V_{eff} values at the location ρ = 2 mm are plotted versus α_d and colored according to discharge current and magnetic field. The data in Fig. 16 display a number of important features:

(1) By all measures, cross-field transport is seen to increase as α_d is decreased, resulting in an order of magnitude change in $\Gamma_\perp$ over the full variation in α_d. Some of the increase in $\Gamma_\perp$ can be ascribed to the increase in edge plasma density as α_d is lowered. However, D_{eff} and V_{eff}, which are not explicitly proportional to *n*, also are found to increase with decreasing α_d, particularly for α_d below ~0.35.

(2) While the magnitude of $\Gamma_\perp$ clearly depends on plasma current (I_p) for a fixed α_d, the transport coefficients, D_{eff} and V_{eff}, are remarkably insensitive to I_p for fixed α_d, much like the behavior of L_n and L_{pe} data in Fig. 12.

(3) Also similar to L_n and L_{pe} in Fig. 12, D_{eff} values appear to exhibit no explicit sensitivity to the toroidal magnetic field strength [panel (c)].

Observations (2) and (3) are consistent with the results shown in Fig. 15; the edge plasma states, including effective transport coefficients, appear to be governed by a quasi-functional dependence on α_d. Yet, one must be careful here. The absolute magnitudes of D_{eff} in Fig. 16 may not be applicable to other tokamaks nor appropriate for input to a generalized transport modeling code. Rather, these D_{eff} values should be considered as merely the flux-gradient relationships found in the stationary states of *these particular discharges* – states which may in fact be fixed by critical beta-gradient boundaries in the phase-space of EMFDT. For example, if one were to change the neutral fueling profile by some external means (via pellet injection, for instance), then a different set of $\Gamma_\perp$, D_{eff} and V_{eff} values may arise, keeping the plasma profiles pinned at roughly the same beta-gradient value. These considerations underscore the inherent difficulty in trying to derive empirical scaling relationships for D_{eff} or V_{eff} in dynamical systems that exhibit a stiff, critical-gradient behavior.

Observation (1) is essentially the increase in cross-field transport with $\bar{n}_e / n_G$ that was detected previously in C-Mod [5, 16], but now parameterized according to α_d in the near SOL. Figure 17 shows that there is indeed a correlation between α_d at $\rho = 2$ mm and $\bar{n}_e / n_G$. Lacking information about α_d near the separatrix, one could in principle use some function of $\bar{n}_e / n_G$ as a rough proxy for this parameter.

Taken together, these data provide some insight into the edge plasma's evolution towards the density limit. In response to increasing $\bar{n}_e / n_G$, the near SOL plasma becomes more dense, more collisional, and evolves toward lower α_d (i.e., smaller $\lambda_{ei} / q^2 R$). Consequently, it can no longer support large normalized beta gradients (Fig. 15). The concomitant increase in neutral ionization source at the edge (arising from the programmed increase in edge neutral density that is used to raise the plasma density) is matched by a dramatic increase in the cross-field particle fluxes (Fig. 16). As a result, α_{MHD} is constrained to lie along a trajectory that is roughly proportional to α_d, for $\alpha_d < \sim 0.35$. However, the rapid growth in cross-field particle fluxes with decreasing α_d cannot continue without limit; at some point one would expect the associated cross-field heat convection to impact the power balance of the discharge, leading to a collapse of the temperature profile.

5.6. Cross-field heat convection

Cross-field heat convection in high density discharges and its connection to the density limit has also been studied previously on C-Mod [5, 16]. Here, we expand the analysis to a wider parameter range and explore the role of α_d as an underlying control parameter.

As outlined in earlier publications [5, 15, 16], it is possible to track the evolution of three key SOL power flows directly from experimental measurements: (1) total power flowing into the

SOL, P_{sol}, (2) power associated with heat convection across the separatix, Q_{conv}, and (3) power conducted along field lines into the divertor region, Q_{div}. The first quantity is simply the input power minus the radiation inside the last-closed flux surface, $P_{sol} = P_{in} - P_{rad}$. The second quantity is derived from an estimate of the particle flux density at the separatrix ($\Gamma_{\perp 0}$) using the particle balance model described in the previous section, $Q_{conv} \sim 5T_{e0}\Gamma_{\perp 0}A_{sep}$, where A_{sep} is the area of the last closed flux surface and T_{e0} is the corresponding electron temperature ($T_{i0} \approx T_{e0}$ is assumed). The third quantity, Q_{div}, is derived from T_e profile measurements. Since parallel electron heat flux is a function of T_e only, i.e., $q_{//} = -\frac{2}{7}\kappa_0 \nabla_{//} T_e^{7/2}$ ($\kappa_0 \approx 2.8\text{x}10^3$ in units of watts m^{-1} $eV^{-7/2}$), a simple estimate of Q_{div} can be obtained by performing the integral [5],

$$Q_{div} \approx A_{sep}\frac{4}{7}\frac{\kappa_0}{\pi^2 R^2 q^2}\int_0^{\rho_{max}}\left(T_e^{7/2} - T_d^{7/2}\right)\partial\rho' . \qquad (1)$$

This formulation is insensitive to the value of ρ_{max} (i.e., the location of the main-chamber limiter) since the integrand decreases rapidly with ρ. Here, we set electron temperature at the divertor surface, T_d, to zero, yielding an upper estimate of Q_{div}.

The three power flows, normalized to the total power into the discharge, are plotted in Fig. 18 – versus $\bar{n}_e / n_G$ in panel (a) and versus α_d in panel (b) – for the full set of ohmic L-mode discharges. Plasma currents of 0.53, 0.8 and 1.0 MA are indicated by symbol shape. It should be noted that P_{in} in these ohmic discharges is roughly proportional to plasma current. Nevertheless, the normalized powers are seen cluster towards the a set of characteristic curves in Fig. 18.

Panel (a) essentially reproduces the trends seen Fig. 6 of Ref. [16] (a data set with $I_p = 0.8$ MA, $B_T = 5.3$ T), but now expands the observations to include the wider I_p and B_T range. As

$\bar{n}_e / n_G$ is increased, a systematic change-over in the SOL power balance is evident: At low values of $\bar{n}_e / n_G$, Q_{div} approximately accounts for P_{sol}. However, as $\bar{n}_e / n_G$ is raised, Q_{conv} rises and Q_{div} no longer accounts for the power into the SOL. An increasing fraction of P_{sol} is carried onto the main-chamber walls via cross-field convection.

The reduction in parallel heat flux to the divertor also appears to affect the onset of divertor detachment; the outer divertor typically detaches when $\bar{n}_e / n_G$ exceeds ~0.32 for I_p= 0.8 MA. Discharges with I_p= 0.53 MA tend to exhibit divertor detachment at slightly lower values, $\bar{n}_e / n_G >$ ~0.27. Correspondingly, the downward-pointing green triangles (I_p= 0.53 MA) are systematically lower than the green diamonds (I_p= 0.8 MA) in Fig. 18a. Thus, while the value of $\bar{n}_e / n_G$ may be used as a rough guide, it is certainly not a unique predictor of the overall edge plasma state.

For large values of $\bar{n}_e / n_G$, cross-field convection to main-chamber structures becomes a dominant power loss mechanism in the SOL. The concomitant growth of cross-field transport with increasing discharge density is highly suggestive; it appears to be a fundamental ingredient in the empirically observed tokamak density limit.

Panel (b) of Fig. 18 tells a similar story, but parameterized in terms of α_d. However, unlike in panel (a), a tight grouping of the green Q_{div} data points is exhibited for $\alpha_d <$ ~0.3, accommodating both I_p= 0.53 and 0.8 MA discharges. As a result, the ratio Q_{div} / P_{in} appears as a monotonic function of α_d in this parameter range, with a remarkably good correlation. Note that the estimate of Q_{div} involves only T_e profile measurements via Eq. (1). Thus, the quasi-functional relationship that is observed here between Q_{div} and α_d is independent of the other ones that are found in these studies: L_{pe} (or L_n) versus α_d in Fig. 12, α_{MHD} versus α_d in Fig.

15, or D_{eff} versus α_d in Fig. 16.

In summary, SOL power balance analysis strongly supports the notion that electromagnetic fluid drift turbulence controls the edge plasma state; the relative balance of parallel and cross-field power flows in the SOL appears to be closely tied to the EMFDT parameter, α_d (or equivalently C_0). Moreover, the observation of a rapid shift from parallel conduction to cross-field convection-dominated heat transport regimes with decreasing α_d (i.e., increasing $\bar{n}_e / n_G$) is entirely consistent with EMFDT playing a central role in tokamak density limit physics.

6. Discussion

6.1. Connection to other scrape-off layer scaling studies

Results from the present study clearly supersede those from earlier transport scaling experiments in Alcator C-Mod [5, 15, 16, 62-64] in terms of data quality and range of discharge parameters. Clear connections between the edge plasma state in C-Mod and the transport paradigm of EMFDT are now evident, in part because flux-gradient relationships in the near SOL are treated separately from those in the far SOL. Nevertheless, the earlier C-Mod research uncovered many features that are reproduced in the present study. Empirical scaling studies on other tokamaks have also uncovered trends similar to those reported here. While not meant to be an exhaustive list, the following commonalities are noteworthy:

(1) *Scrape-off widths and transport levels increase with increasing edge plasma collisionality.* Experiments on ASDEX [65] were perhaps the first to note a strong reduction in SOL width as the local electron temperature was increased. Similar trends were later noted in C-Mod [64, 66], JT-60U [67] and JET [68] as well as correlated

with plasma collisionality and $\bar{n}_e / n_G$ in ASDEX Upgrade [69, 70] and C-Mod [5, 15, 16].

(2) *Scrape-off widths and transport levels are insensitive to toroidal magnetic field.* Contrary to the then prevailing expectations of a Bohm transport scaling, results from C-Mod [64] and JET [68] indicated no dependence of SOL widths and transport on the value of the magnetic field strength. Scaling studies focusing on L-mode discharges from a larger set of tokamaks indicated similar trends [71-73].

(3) *Evidence for critical beta-gradient behavior.* The lack of a toroidal magnetic field scaling in the inferred cross-field transport pointed to a critical poloidal beta-gradient (α_{MHD}) model as one of several possible candidates for L-mode SOLs [71, 72]. Scaling studies on ASDEX Upgrade noted that pressure gradient e-folding lengths in the edge of H-modes tend to scale as $L_{nTe} \sim n / I_p^2$ [73] with heat diffusivities scaling similarly [70]. These observations are largely consistent with α_{MHD} defining the operational boundaries of the discharge via pressure gradient driven instabilities [69]. Possible connections to the empirical density limit were also noted in these studies. H-mode pedestal scaling studies on Alcator C-Mod have also found edge pressure gradients to be proportional to I_p^2 with lack of any B_T dependence [1]. The latter results make direct contact with the data presented here and imply that critical poloidal beta-gradients set both the L-mode and H-mode edge plasma states in Alcator C-Mod. As recounted by Neuhauser [20], the full range of edge plasma experiences on ASDEX and ASDEX Upgrade is entirely consistent with a critical-gradient transport paradigm, both for the behavior of the steep-gradient region near the separatrix and the rapid

transport region in the far SOL – observations that resonate with others reviewed in section 2.

(4) *Extension of the H-mode transport barrier into the SOL.* Evidence of the H-mode pedestal extending into the near SOL has been seen previously in C-Mod [64] and noted most recently in JET [74], while intermittent transport is found to persist in the far SOL, albeit at a reduced overall levels [24, 75]. These results imply that the turbulence suppression mechanism of the H-mode also extends into the near SOL. It is interesting to note that, independent of L or H regime, the location of the pressure profile's minimum in L_{pe} tends to reside in the near SOL. Building on these observations, one might further speculate that plasma conditions in the near SOL are actively involved in triggering the H-mode, perhaps via access to a more stable region in α_{MHD}-α_d space – a scenario that is somewhat suggested by the data in Fig. 15 in conjunction with the theoretical ideas discussed in section 5.4.

6.2 Potential role of plasma flow shear

One topic that deserves further investigation is the role of edge flows. For example, does plasma flow shear affect the mapping of achievable edge plasma states in α_{MHD}-α_d space? Recent experiments have uncovered connections between transport-driven edge plasma flows and the input power required to trigger an H-mode [40, 76]. These results indicate that scrape-off layer flows do indeed exhibit stronger shear in magnetic topologies that favor H-modes. Correspondingly, subtle but noticeable differences in L-mode plasma pressure profiles are evident in the near SOL, with tendencies for higher α_{MHD} in discharges with lower L-H power thresholds. Similar differences were noted earlier in forward versus reversed magnetic field

discharges on C-Mod [77]. Unfortunately, the latter results need to verified; they were obtained over several months of tokamak operation with potentially degrading probe diagnostics. We hope to report more results on this topic in the future.

6.3 Comments on power-law regression analysis

Power-law regression analysis, which is often used to look for intrinsic scalings among physical parameters in experiments, was not used in this paper. Clearly, a simple power-law expression would not be capable of representing the quasi-functional dependences on α_d that are detected (e.g. Figs. 15 and 16). In this sense, our use of power-law fits in previous investigations [5, 15, 16, 62-64] was a bit misleading; data at both low and high values of α_d were scrambled into one large dataset to be fit. Although important trends were indeed uncovered (sensitivity of transport to λ_{ei}/qR, for example), the resultant power-law exponents should, in retrospect, be treated with caution. These comments should serve as a warning to others who perform similar empirical scaling analyses over a wide range of operational space.

7. Summary

Plasma conditions in the 'near scrape-off layer', a region ~2 mm outside the last closed flux surface, are examined in Alcator C-Mod for a wide range of plasma currents, toroidal fields and densities in ohmic L-mode discharges. A smaller set of ohmic H-mode discharges are also studied. By a number of separate measures (summarized below), these data reveal strong evidence that electromagnetic fluid drift turbulence (EMFDT) determines the locus of edge states that are accessible to the plasma, i.e., the self-consistent combinations of plasma density,

temperature, gradients and fluxes that satisfy particle and power balance constraints.

(1) Plasma collisionality, as defined within the framework of EMFDT (see Table 1), is found to determine the overall edge plasma state. Density and pressure gradient scale lengths track monotonic functions of C_0 or α_d; data from a wide range of currents, fields and densities tend to coalesce onto a single quasi-functional dependence of the dimensionless grouping, λ_{ei}/q^2R, which is contained within the parameters C_0 and α_d.

(2) Normalized plasma pressure gradients ($\hat{\beta}$ or α_{MHD}) are also found to behave in a way that is consistent with the physics of EMFDT: for fixed values of C_0 or α_d, absolute pressure gradients scale as I_p^2, rendering $\hat{\beta}$ or α_{MHD} unchanged. Thus, the observed edge plasma states cluster towards a characteristic curve in the dimensionless phase-space of EMFDT. The overall behavior is suggestive of a critical-gradient (i.e. α_{MHD}) transport paradigm – a model that is consistent with cross-field transport being insensitive to toroidal field strength, as detected in previous studies.

(3) Cross-field transport (i.e. particle fluxes, effective particle diffusivities and/or convection) is found to increase dramatically with decreasing α_d (or increasing C_0) for the range α_d < ~0.35, with effective cross-field particle diffusivities exhibiting a quasi-functional dependence on α_d. This near-explosive growth of cross-field transport with increasing collisionality roughly corresponds to the location in α_{MHD}-α_d space where a 'density-limit boundary' is thought to occur, based on EMFDT simulations [9, 14, 60]. Edge plasma states are observed to cluster along this 'density-limit boundary' with α_{MHD} roughly proportional to α_d, for α_d < ~0.35. The behavior is consistent with edge states being constrained to satisfy particle and energy balance in addition to EMFDT transport

physics.

(4) At low values of α_d, cross-field heat convection to the main-chamber walls is seen to compete with parallel electron conduction to the divertor region, helping to precipitate divertor detachment and impacting the overall power flow through the edge. α_d is found to be a better predictor than $\bar{n}_e / n_G$ in parameterizing this thermal collapse; heat flow into the divertor normalized to the total power into the SOL exhibits (yet another) characteristic quasi-functional dependence on α_d that includes data points from a wide range of plasma currents, toroidal fields and densities. These observations strongly support the notion that the empirical density limit in tokamaks is fundamentally a transport limit, largely imposed by the physics of EMFDT.

(5) For values of α_d exceeding ~0.35, ohmic L-mode states with α_{MHD} above the parametric line, $\alpha_{MHD} \approx 0.15/\alpha_d^2$ do not appear to be accessible. In addition, ohmic L-modes that lie near this line with $\alpha_d >$ ~0.5 are seen to spontaneously transition to ohmic H-modes. After transition, the edge states evolve toward increased α_{MHD} and decreased α_d values. While somewhat speculative, these observations make contact with an idea that the L-H threshold is an intrinsic part of EMFDT physics: once the edge plasma state crosses a critical boundary in α_{MHD}-α_d space, turbulence may be suppressed, causing a spontaneous transition into H-mode [9, 57]. It is interesting to note that the parametric boundary line, $\alpha_{MHD} \approx 0.15/\alpha_d^2$, is functionally identical to the H-mode threshold condition proposed by Guzdar [57].

In aggregate, the above observations form a compelling collection of evidence. Electromagnetic fluid drift turbulence, as studied by the turbulence simulation work of Scott [8],

RDZ [9], and Xu [60], does indeed appear to control the edge plasma state in the Alcator C-Mod tokamak. While the focus in this paper is mostly on L-mode discharges, a number of similarities exist between the scalings uncovered here and those published previously for the H-mode pedestal in Alcator C-Mod [1], most notably the scaling of pedestal pressure gradients with I_p^2.

Finally, if nothing else, the overall behavior of the edge plasma system observed in these experiments should be retained. The range of allowed edge plasma states is constrained to well-defined regions in the phase-space of EMFDT. This behavior is indicative of a marginally-stable system, where small changes in poloidal beta gradient lead to large changes in transport fluxes. Thus, the appropriate transport paradigm appears to be closer to a 'self-organized critical' system than a 'simple diffusive transport' system – energy and particle fluxes are externally imposed; gradients adjust themselves to satisfy marginal stability constraints; effective diffusion coefficients are 'adjusted' by the dynamics to match the two. Such a dynamical system is precisely what is needed to explain the intermittent, avalanche-like transport phenomena observed in the far SOL. Yet, the near SOL plays the more dominant role; it determines the level of particle and heat input that is required to reach the desired plasma conditions just inside the last closed flux surface.

Acknowledgements

Alcator C-Mod's contributions to fusion energy science are made possible by the excellent engineers, technical staff, students, and scientists on the Alcator team. We wish to acknowledge valuable discussions with Olaf Grulke, Parvez Guzdar, Barrett Rogers, Bruce Scott, Maxim Umansky, Xueqiao Xu, and Stewart Zweben. This work is supported by U.S. Department of Energy Coop. Agreement DE-FC02-99ER54512.

References

[1] Hughes, J.W., Mossessian, D.A., Hubbard, A.E., LaBombard, B., and Marmar, E.S., Phys. Plasmas **9** (2002) 3019.

[2] Osborne, T.H., et al., Plasma Phys. Control. Fusion **40** (1998) 845.

[3] Suttrop, W., et al., Plasma Phys. Control. Fusion **39** (1997) 2051.

[4] Pitcher, C.S., et al., Phys. Plasmas **4** (1997) 2577.

[5] LaBombard, B., et al., Phys. Plasmas **8** (2001) 2107.

[6] Zeiler, A., *Tokamak Edge Turbulence*, Max-Planck-Institut für Plasmaphysik Research Report: IPP 5/88, July 1999,

[7] Scott, B., *Low frequency fluid drift turbulence in magnetised plasmas*, Max-Planck-Institut für Plasmaphysik Research Report: IPP 5/92, March 2001,

[8] Scott, B., Plasma Phys. Control. Fusion **39** (1997) 1635.

[9] Rogers, B.N., Drake, J.F., and Zeiler, A., Phys. Rev. Lett. **81** (1998) 4396.

[10] Xu, X.Q., et al., J. Nucl. Mater. **266** (1999) 993.

[11] Braginskii, S.I., in Reviews of Plasma Physics (1965), Consultants Bureau, New York Vol. 1, 205.

[12] Xu, X.Q., et al., Nucl. Fusion **40** (2000) 731.

[13] Myra, J.R., D'lppolito, D.A., Xu, X.Q., and Cohen, R.H., Phys. Plasmas **7** (2000) 4622.

[14] Xu, X.Q., et al., in Fusion Energy 2004: Proc. 20th Int. Conf. (Vilamoura, 2004), (Vienna: IAEA), CD ROM file TH1_5 and http://www.iaea.org/programmes/ripc/physics/fec2004/html/fec2004.htm.

[15] LaBombard, B., et al., Nucl. Fusion **40** (2000) 2041.

[16] LaBombard, B., et al., in Fusion Energy 2002: Proc. 19th Int. Conf. (Lyon, 2002), (Vienna: IAEA), CD ROM file EXD2_1 and http://www.iaea.org/programmes/ripc/physics/fec2002/html/fec2002.htm.

[17] Carreras, B.A., to be published in the Journal of Nuclear Materials (2005).

[18] Endler, M., et al., Nucl. Fusion **35** (1995) 1307.

[19] Boedo, J.A., et al., Phys. Plasmas **8** (2001) 4826.

[20] Neuhauser, J., et al., Plasma Phys. Control. Fusion **44** (2002) 855.

[21] Rudakov, L., et al., Plasma Phys. Control. Fusion **44** (2002) 717.

[22] Hidalgo, C., et al., J. Nucl. Mater. **313-316** (2003) 863.

[23] Boedo, J.A., et al., J. Nucl. Mater. **313-316** (2003) 813.

[24] Boedo, J.A., et al., Phys. Plasmas **10** (2003) 1670.

[25] Antar, G.Y., Counsell, G., Yang, Y., Labombard, B., and Devynck, P., Phys. Plasmas **10**

(2003) 419.

[26] Zweben, S.J., et al., Phys. Plasmas **9** (2002) 1981.

[27] Terry, J.L., et al., Phys. Plasmas **10** (2003) 1739.

[28] Zweben, S.J., et al., Nucl. Fusion **44** (2004) 134.

[29] Carreras, B.A., et al., Phys. Rev. Lett. **80** (1998) 4438.

[30] Sarazin, Y. and Ghendrih, P., Phys. Plasmas **5** (1998) 4214.

[31] Maqueda, R.J., et al., Bull. Amer. Phys. Soc. **49** (2004).

[32] Endler, M., et al., Plasma Phys. Control. Fusion **47** (2005) 219.

[33] Greenwald, M., et al., Phys. Plasmas **6** (1999) 1943.

[34] Hubbard, A.E., et al., Phys. Plasmas **8** (2001) 2033.

[35] Krasheninnikov, S.I., Phys. Rev. A **283** (2001) 368.

[36] Fundamenski, W. and Sailer, W., Plasma Phys. Control. Fusion **46** (2004) 233.

[37] Ghendrih, P., et al., J. Nucl. Mater. **313-316** (2003) 914.

[38] D'Ippolito, D.A., Myra, J.R., and Krasheninnikov, S.I., Phys. Plasmas **9** (2002) 222.

[39] Umansky, M.V., Krasheninnikov, S.I., LaBombard, B., and Terry, J.L., Phys. Plasmas **5** (1998) 3373.

[40] LaBombard, B., et al., Nucl. Fusion **44** (2004) 1047.

[41] Hutchinson, I.H., et al., Phys. Plasmas **1** (1994) 1511.

[42] Hughes, J.W., et al., Rev. Sci. Instrum. **72** (2001) 1107.

[43] LaBombard, B., Phys. Plasmas **9** (2002) 1300.

[44] Boivin, R.L., et al., Phys. Plasmas **7** (2000) 1919.

[45] Granetz, R.S., Hutchinson, I.H., Gerolamo, J., Pina, W., and Tsui, C., Rev. Sci. Instrum. **61** (1990) 2967.

[46] Lao, L.L., et al., Nucl. Fusion **25** (1985) 1611.

[47] Greenwald, M., et al., Nucl. Fusion **28** (1988) 2199.

[48] Gangadhara, S. and LaBombard, B., Plasma Phys. Control. Fusion **46** (2004) 1617.

[49] Greenwald, M., Plasma Phys. Control. Fusion **44** (2002) 27.

[50] Stek, P., *Reflectometry Measurements on Alcator C-Mod*, PhD Thesis (Cambridge: MIT) 1997, Research Report: PSFC/RR-97-5, http://psfcwww2.psfc.mit.edu/library/97rr/97rr005/97rr005_abs.html.

[51] Lin, Y., et al., Rev. Sci. Instrum. **70** (1999) 1078.

[52] Snipes, J.A., et al., Plasma Phys. Control. Fusion **43** (2001) L23.

[53] Scott, B.D., New Journal of Physics **4** (2002).

[54] Rogers, B.N. and Drake, J.F., Phys. Rev. Lett. **79** (1997) 229.

[55] Zeiler, A., Biskamp, D., Drake, J.F., and Guzdar, P.N., Phys. Plasmas **3** (1996) 2951.

[56] Guzdar, P.N., Drake, J.F., McCarthy, D., Hassam, A.B., and Liu, C.S., Phys. Fluids **5** (1993) 3712.

[57] Guzdar, P.N., Kleva, R.G., Das, A., and Kaw, P.K., Phys. Rev. Lett. **87** (2001) 015001.

[58] Guzdar, P.N., Kleva, R.G., Groebner, R.J., and Gohil, P., Phys. Rev. Lett. **89** (2002) 265004.

[59] Hubbard, A.E., et al., Plasma Phys. Control. Fusion **46** (2004) A95.

[60] Xu, X.Q., et al., Phys. Plasmas **10** (2003) 1773.

[61] Hubbard, A.E., et al., Plasma Phys. Control. Fusion **40** (1998) 689.

[62] LaBombard, B., et al., Phys. Plasmas **2** (1995) 2242.

[63] LaBombard, B., et al., in Plasma Physics and Controlled Fusion Research 1996 (Proc. 16th Int. Conf. Montreal, 1996), IAEA, Vienna (1997) Vol. 1, 825.

[64] LaBombard, B., et al., J. Nucl. Mater. **241-243** (1997) 149.

[65] McCormick, K., et al., J. Nucl. Mater. **196-198** (1992) 264.

[66] LaBombard, B., Jablonski, D., Lipschultz, B., McCracken, G., and Goetz, J., J. Nucl. Mater. **220-222** (1995) 976.

[67] Asakura, N., et al., J. Nucl. Mater. **241-243** (1997) 559.

[68] Erents, S.K. and Stangeby, P.C., Nucl. Fusion **38** (1998) 1637.

[69] Suttrop, W., Mertens, V., Murmann, H., Neuhauser, J., and Schweinzer, J., J. Nucl. Mater. **266-269** (1999) 118.

[70] Kim, J.W., Coster, D.P., Neuhauser, J., and Schneider, R., J. Nucl. Mater. **290-293** (2001) 644.

[71] Connor, J.W., et al., Nucl. Fusion **39** (1999) 169.

[72] Counsell, G.F., et al., J. Nucl. Mater. **266-269** (1999) 91.

[73] McCormick, K., et al., J. Nucl. Mater. **266-269** (1999) 99.

[74] Fundamenski, W. and Sipila, S., Nucl. Fusion **44** (2004) 20.

[75] Terry, J.L., et al., J. Nucl. Mater. **290** (2001) 757.

[76] LaBombard, B., et al., Phys. Plasmas **12** (2005) 056111.

[77] LaBombard, B., Hughes, J., Greenwald, M., Mossessian, D., and Terry, J.L., Bull. Am. Phys. Soc. **48** (2003) 52.

Table 1. Definitions, normalizations, and key dimensionless control parameters for electromagnetic fluid drift turbulence (EMFDT), as identified in the work of Rogers, Drake, Zeiler, *et al.* (RDZ [9,54,55]) and Scott [8,53]. Note that $p_e \equiv nT_e$ and the approximation $T_{i0} \approx T_{e0}$ is used to simplify the expressions.

	RDZ	**Scott**
	Definitions and Normalizations	
Time $\frac{\partial}{\partial t} \sim \frac{1}{t_0}$	Ideal Ballooning Time $t_0 = \left(\frac{RL_n}{2}\right)^{1/2} \frac{1}{C_s}$	Drift Scaling $t_0 = \frac{L_{Pe}}{C_s}$
Perpendicular $\nabla_\perp \sim \frac{1}{L}$	Linear Resistive Ballooning Scale $L = L_0 = 2\pi q \left(\frac{\rho_s \rho_e R}{\lambda_{ei}}\right)^{1/2} \left(\frac{2R}{L_n}\right)^{1/4}$	$L = \rho_s$
Parallel $\nabla_{//} \sim \frac{1}{L_{//}}$	$L_{//} = 2\pi qR$	$L_{//} = qR$
Background Gradients	$\frac{\nabla_\perp n_0}{n_0} \sim \frac{1}{L_n}$; $\frac{\nabla_\perp T_{e0}}{T_{e0}} \sim \frac{1}{L_{Te}}$; $\frac{\nabla_\perp T_{i0}}{T_{i0}} \sim \frac{1}{L_{Ti}}$; $\frac{\nabla_\perp p_{e0}}{p_{e0}} \sim \frac{1}{L_{Pe}}$	
	Key Control Parameters	
Poloidal Beta Gradient	MHD Ballooning Parameter $\alpha_{MHD} = \frac{q^2 R}{L_{Pe}} \beta$; $\beta = \frac{4\mu_0 p_{e0}}{B^2}$	$\hat{\beta} = \frac{q^2 R}{L_{Pe}} \beta \left(\frac{R}{4L_{Pe}}\right)$
Collisionality	Drift Frequency/Ballooning Time $\alpha_d = \frac{T_{e0} t_0}{eBL_n L_0}$ $\alpha_d = \left(\frac{\lambda_{ei}}{q^2 R}\right)^{1/2} \left(\frac{2R}{L_n}\right)^{1/4} \frac{1}{8\pi} \left(\frac{M_i}{m_e}\right)^{1/4}$	Normalized Collision Frequency $C_0 = \frac{m_e}{M_i} \left(\frac{qR}{L_{Pe}}\right)^2 \frac{\nu_{ei} L_{Pe}}{C_s}$ $C_0 = \left(\frac{q^2 R}{\lambda_{ei}}\right) \left(\frac{R}{L_{Pe}}\right) \left(\frac{m_e}{M_i}\right)^{1/2}$
	Relationships Between Control Parameters	
	$\alpha_{MHD} = \hat{\beta} \frac{4L_{Pe}}{R}$; $\alpha_d = \frac{C_0^{-1/2}}{4\pi} \left(\frac{R}{2L_n}\right)^{1/4} \left(\frac{R}{2L_{Pe}}\right)^{1/2}$	

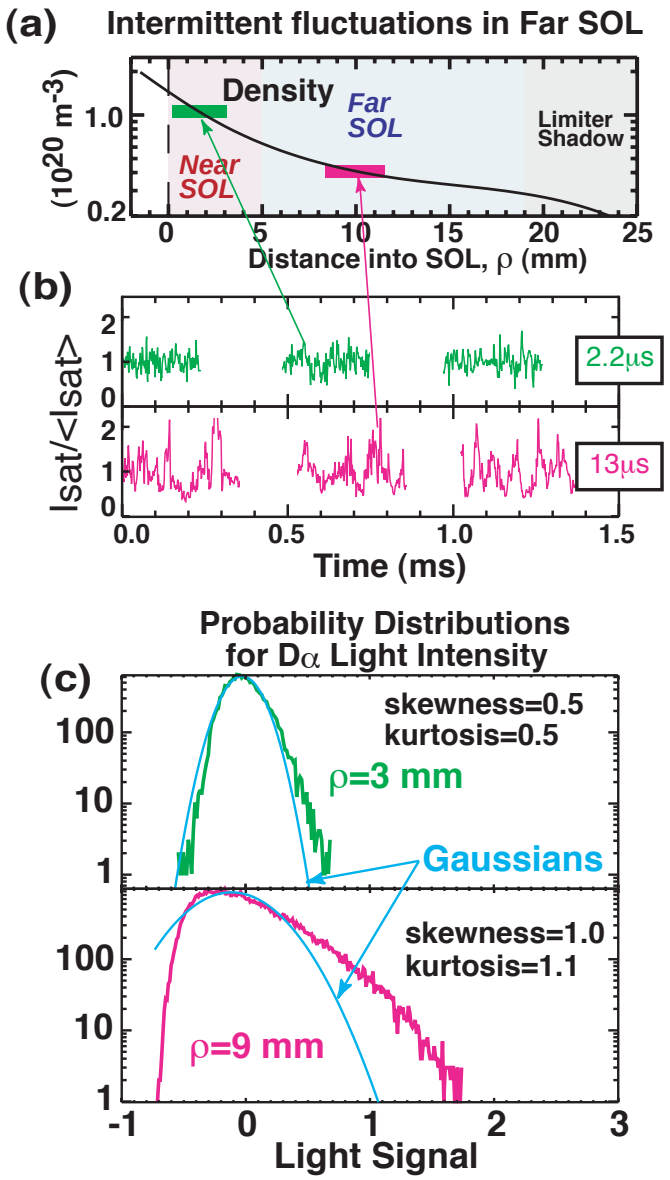

Figure 1. The *near* SOL zone of Alcator C-Mod (ρ < ~5 mm) is characterized by steep gradients while the *far* SOL typically has relatively flattened profiles, as seen in a representative density profile (a). These two zones also exhibit different fluctuation characteristics: low amplitude, near Gaussian fluctuations in the *near* SOL and intermittent, non-Gaussian fluctuations in *far* SOL, as is evident in ion saturation current time signals (b) and in probability distributions of D_α light intensity fluctuations (c). Autocorrelation times for the ion saturation current time signals are indicated in the boxes of (b).

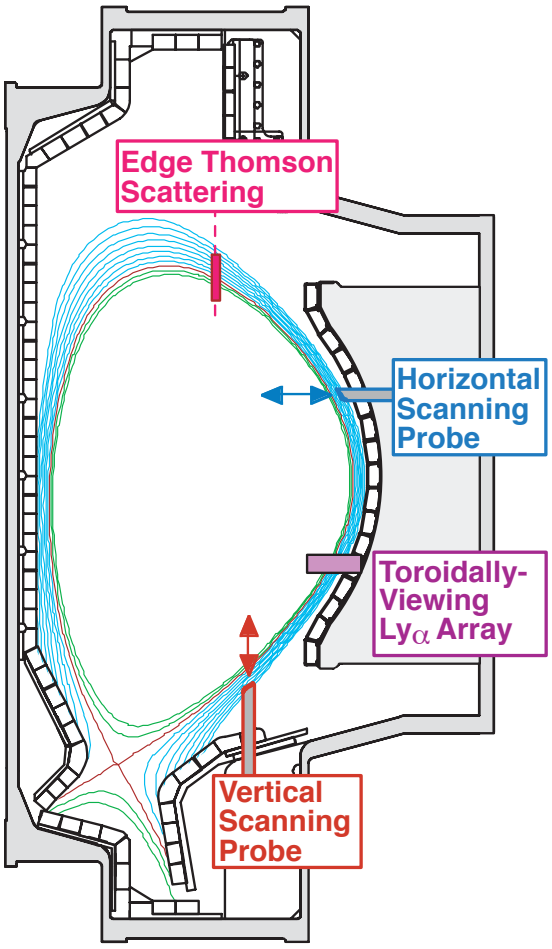

Figure 2. Cross-section of Alcator C-Mod showing locations of key diagnostics used for the present study. High-resolution density and electron temperature profiles across the separatrix and scrape-off layer regions are assembled from edge Thomson scattering and horizontal scanning probe diagnostics. Cross-field plasma fluxes in this region are estimated from a particle balance technique [15], using plasma flow measurements from a vertical probe and ionization profile estimates from a toroidally-viewing Ly_α diagnostic [44].

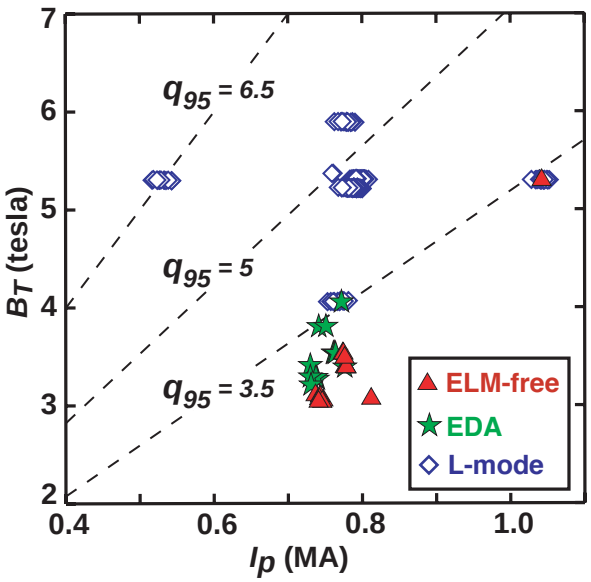

Figure 3. Toroidal magnetic fields (B_T) and plasma currents (I_p) for the discharges under investigation. A density scan was performed in ohmic L-mode discharges at 5 nominal combinations of B_T and I_p, yielding safety factors at the 95% flux surface (q_{95}) of roughly 3.5, 5 and 6.5. ELM-free and EDA Ohmic H-modes were also investigated. These were obtained when q_{95} was reduced below ~3.5.

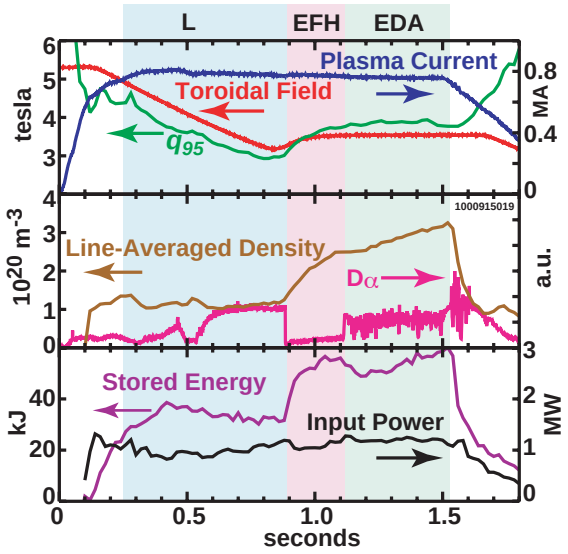

Figure 4. Time history of an ohmic discharge with L-mode (L) and H-mode phases (EFH, EDA). The discharge changes from inner-wall limited to diverted at approximately 0.28 seconds. The toroidal magnetic field is ramped down to promote an L-H transition and subsequently ramped up to a stationary value. A short ELM-free H-mode (EFH) phase is followed by an EDA H-mode phase (EDA).

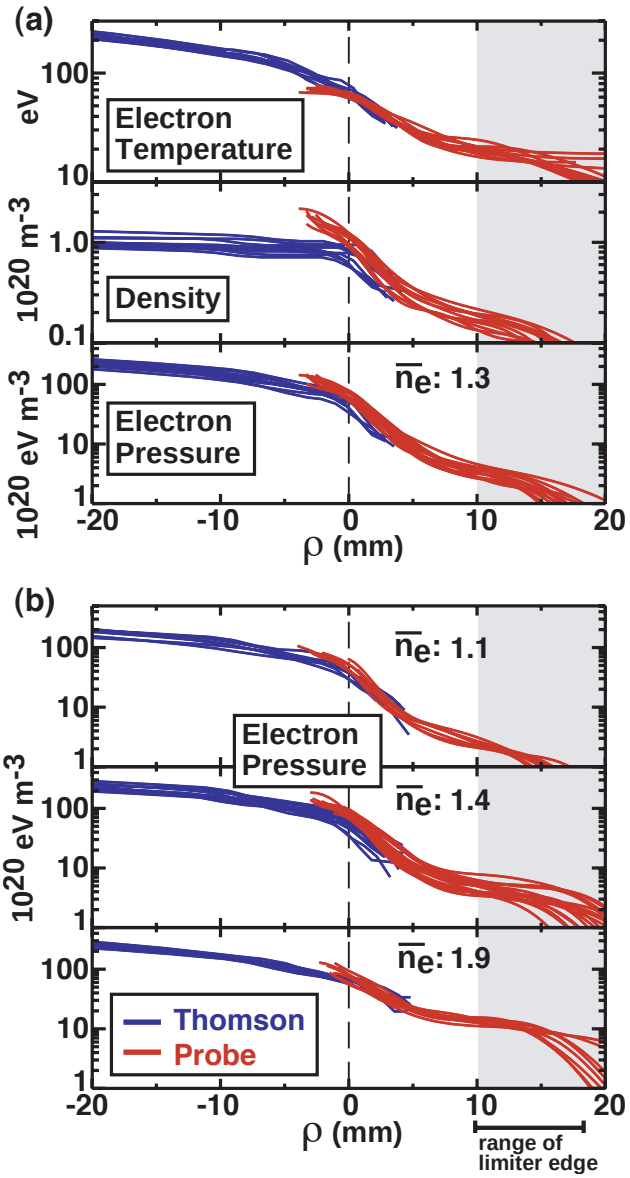

Figure 5. Overlaid profiles of electron temperature (T_e), density (n) and electron pressure ($p_e = nT_e$) measured by the horizontal scanning probe (red) and edge Thomson scattering systems (blue) for ohmic L-mode discharges with B_T = 5.4 T and I_p = 0.8 MA. The flux surface coordinate, ρ, is the distance into the SOL, mapped to the outer midplane. The gray area indicates where field lines may map to a limiter surface for a given profile. The location of the limiter edge varies from profile to profile; the horizontal bar shows the full range of limiter edge locations. As the line-average plasma density is raised ($\bar{n}_e$, in units of 10^{20} m^{-3}), a trend of flattening p_e profiles near $\rho = 0$ is seen on both diagnostics. For $\rho < 0$, the probe-inferred profiles are unreliable. In overlapping spatial regions where both diagnostics operate reliably, the plasma density inferred by the probe also appears to be high relative to that of the Thomson system.

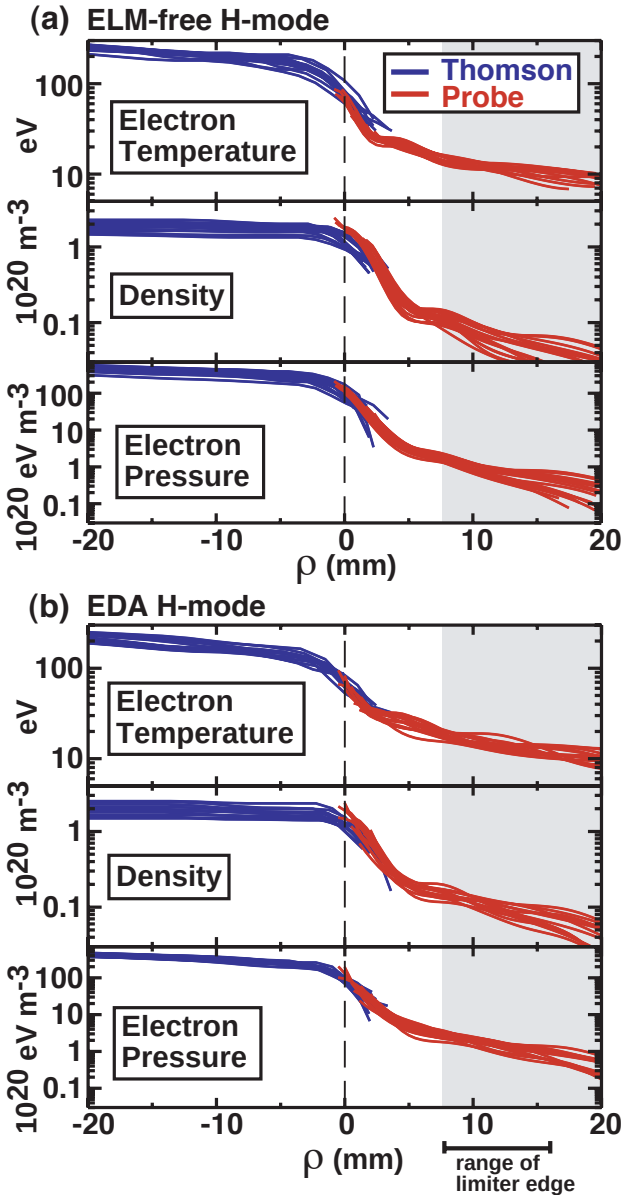

Figure 6. Overlaid profiles from Thomson and probe systems for ELM-free (a) and EDA (b) phases of ohmic H-mode discharges (I_p = ~0.75 MA, B_T = 3.2 to 4 T). The trend of steeper pressure profiles near the separatrix in these discharges tracks well between the two diagnostics.

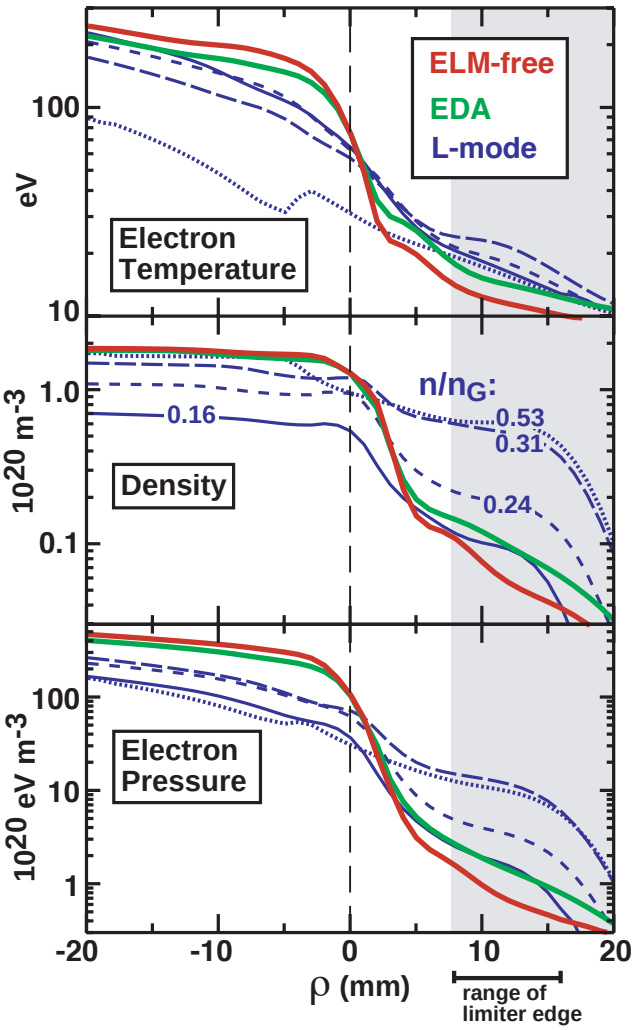

Figure 7. Composite profiles assembled from probe and Thomson data for both ohmic L-mode and H-mode discharges. ELM-free and EDA H-mode profiles correspond to those discharges in Fig. 3 with $0.7 < I_p < 0.8$ MA. Averaged profiles are also shown from ohmic L-mode discharges (I_p = 0.8 MA, B_T = 5.3 T) with four different line-averaged densities ($\bar{n}_e / n_G$ values are indicated).

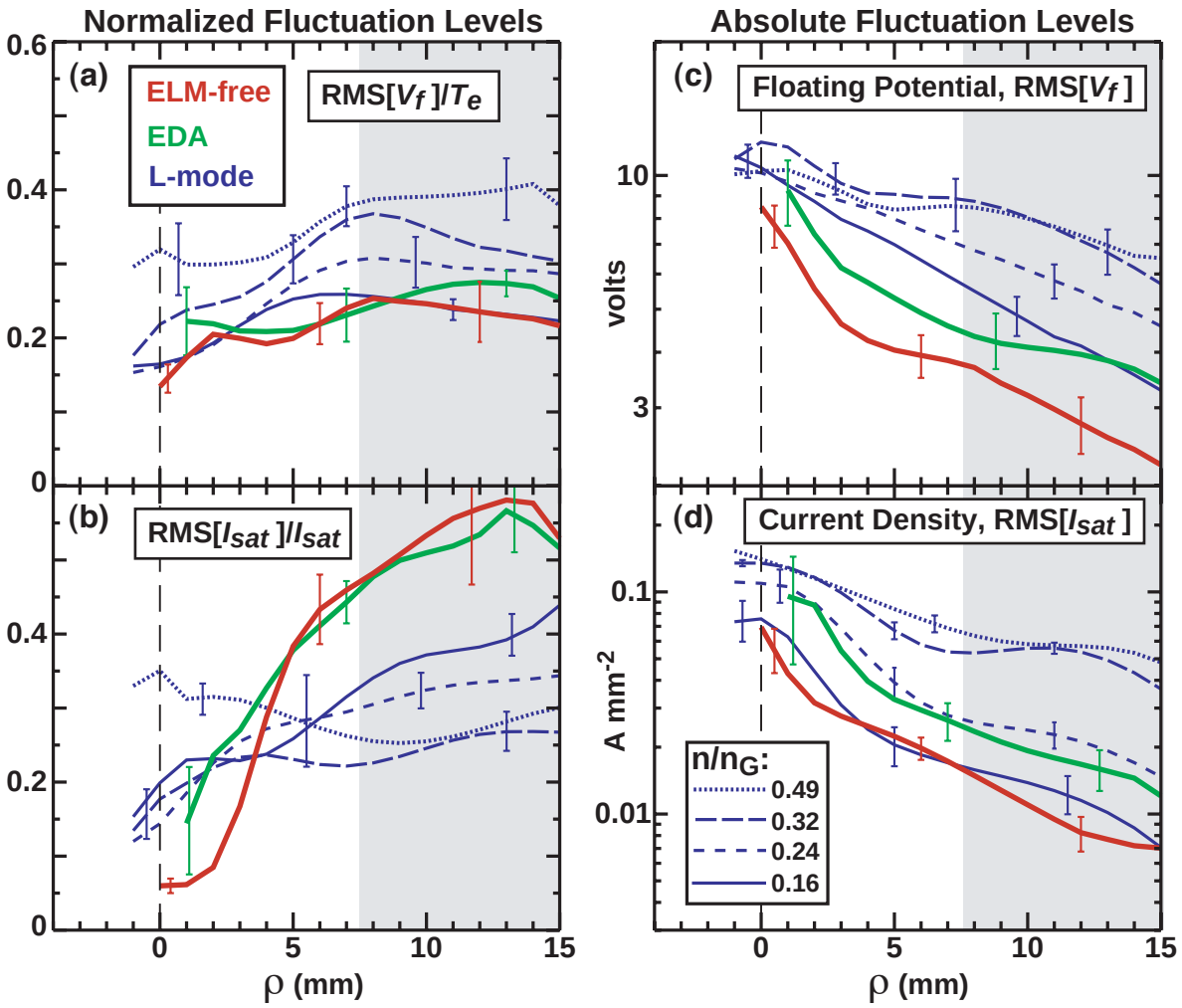

Figure 8. RMS fluctuation amplitudes in floating potential normalized to electron temperature (a) and ion saturation current normalized to its time-averaged value (b) recorded by the horizontal scanning probe. Absolute fluctuation amplitudes are shown in (c) and (d). The curves represent average profiles from a number of plasmas. Vertical bars indicate ±1 standard deviation, computed from the variance among similar plasmas.

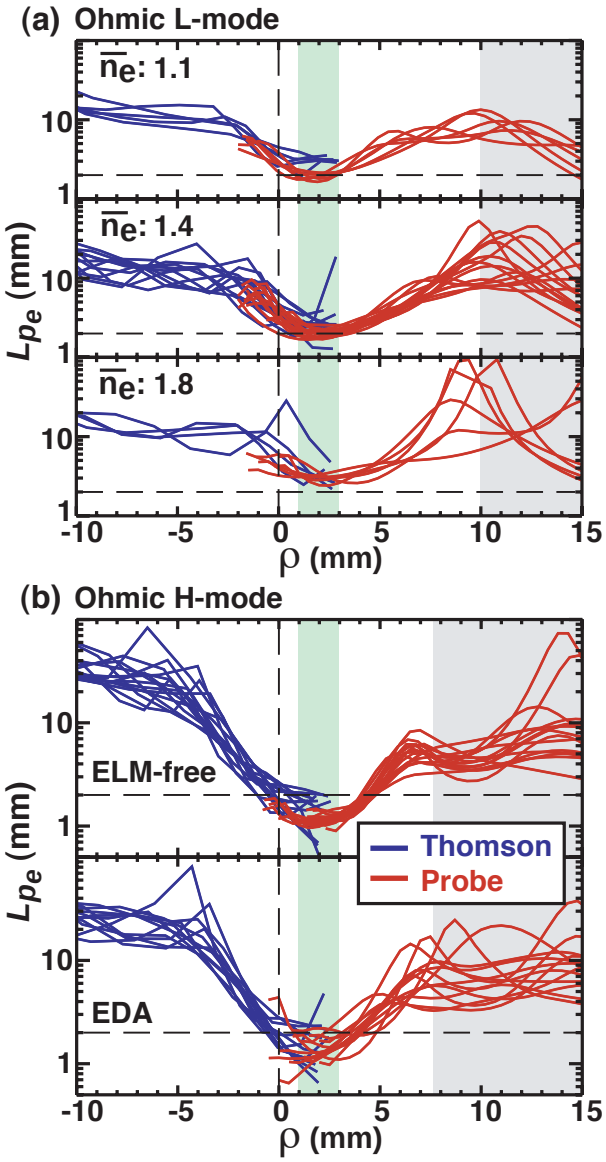

Figure 9. Profiles of electron pressure gradient scale lengths (L_{pe}) as inferred separately from scanning probe and Thomson scattering systems. Both systems report a similar minimum value of L_{pe} in the near SOL, even as L_{pe} at this location is reduced by a factor of ~3 in going from high density L-mode discharges to ELM-free H-mode discharges. The same radial location of the minimum (ρ ~ 2 mm, green band) is observed in all profiles, lending confidence that the discharge-to-discharge variation in the flux surface mapping is within about a 2 mm band.

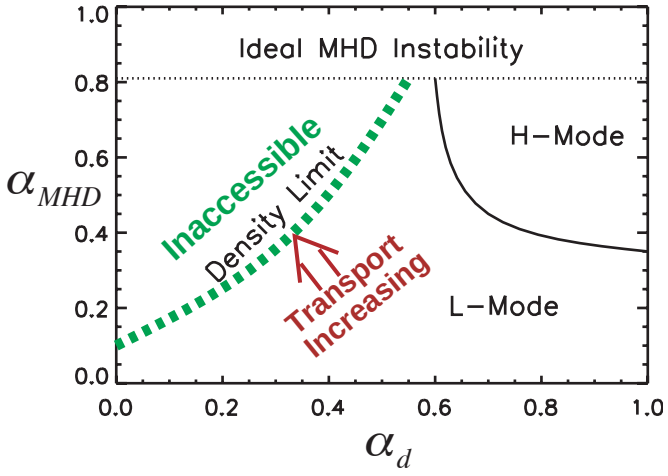

Figure 10. The phase space of EMFDT, as identified in the work of Rodgers, Drake and Zeiler (RDZ [9]). The existence of a transport-defined tokamak 'density limit' was identified with a boundary at high collisionality (small α_d), across which the cross-field transport was observed to increase sharply.

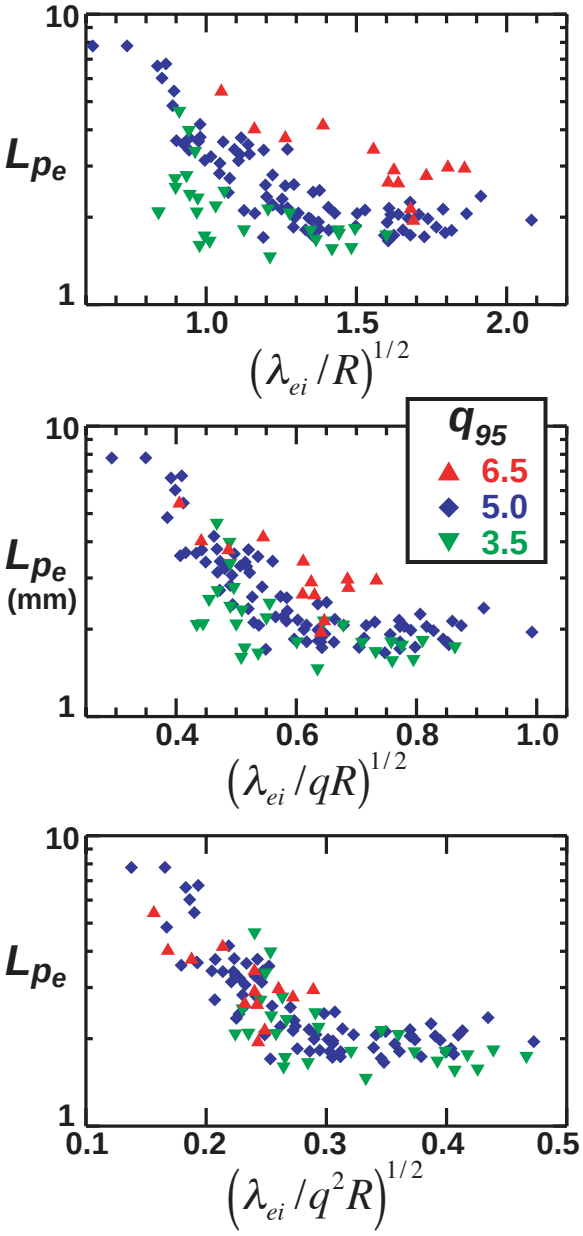

Figure 11. Pressure gradient scale lengths (L_{pe}) at the location ρ = 2 mm in ohmic L-mode discharges, plotted as a function of local plasma collisionality using three different normalizations: (a) electron mean free path (λ_{ei}) normalized to major radius, R, (b) λ_{ei} normalized to magnetic field line connection length, qR, and (c) λ_{ei} normalized to q^2R. The latter normalization does the best job of grouping the L_{pe} data.

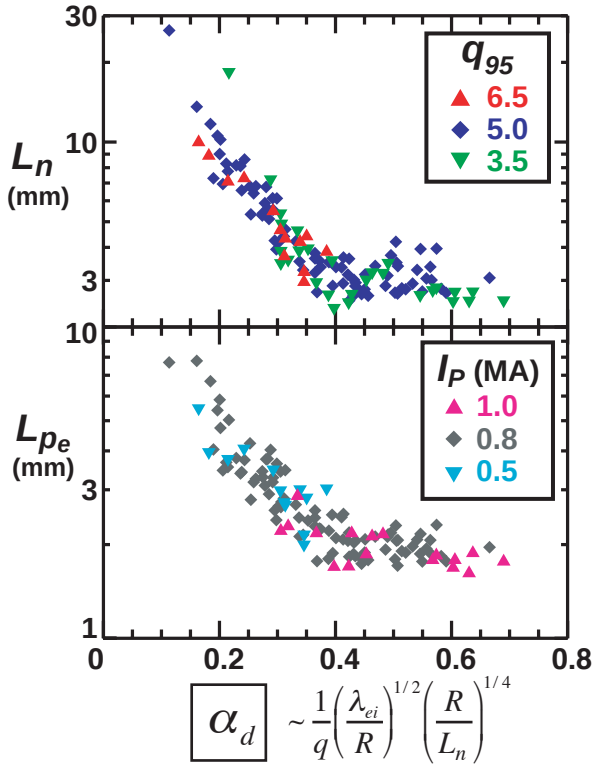

Figure 12. Density and pressure gradient scale lengths at the location ρ = 2 mm in ohmic L-mode discharges, plotted as a function of the local value of the 'diamagnetic parameter', α_d Over a wide range of plasma conditions, the local values of L_n and L_{pe} are found to cluster around a monotonic function of α_d.

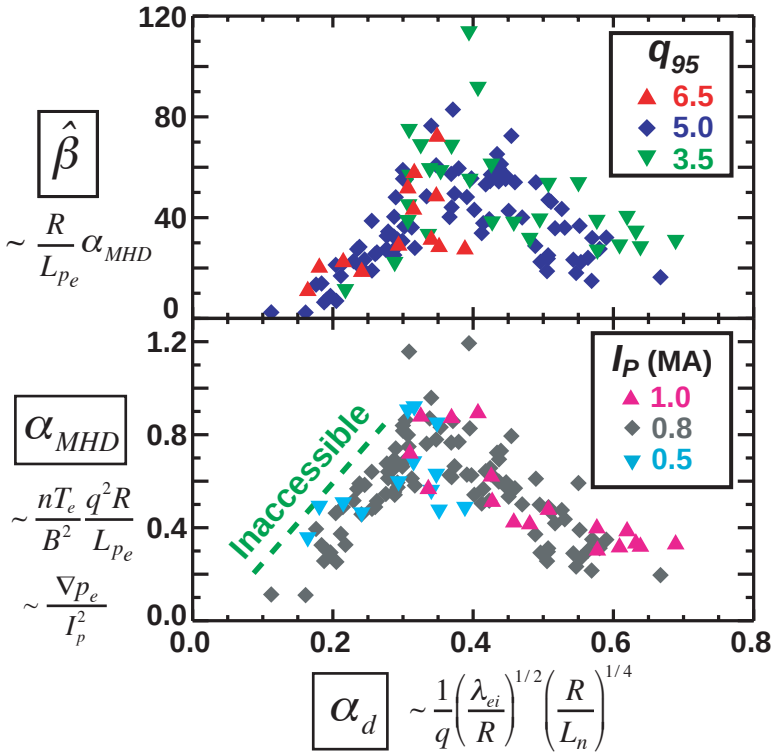

Figure 13. Normalized electron pressure gradients at the location ρ = 2 mm in ohmic L-mode discharges, plotted as a function of α_d. Two different normalizations are used: (a) $\hat{\beta}$ as defined by Scott [8] and (b) α_{MHD}, the MHD ballooning parameter, as used in the work of RDZ [9]. The observed edge plasma states are found to group remarkably well in this two-parameter space – a phase-space that is found to control the level of cross-field transport within the framework of electromagnetic fluid drift turbulence theory. Owing to high cross-field transport (discussed further in sections 5.5 and 5.6), a triangular-shaped region at high α_{MHD} and low α_d is not accessible. This behavior is also consistent with EMFDT simulations (see Fig. 10).

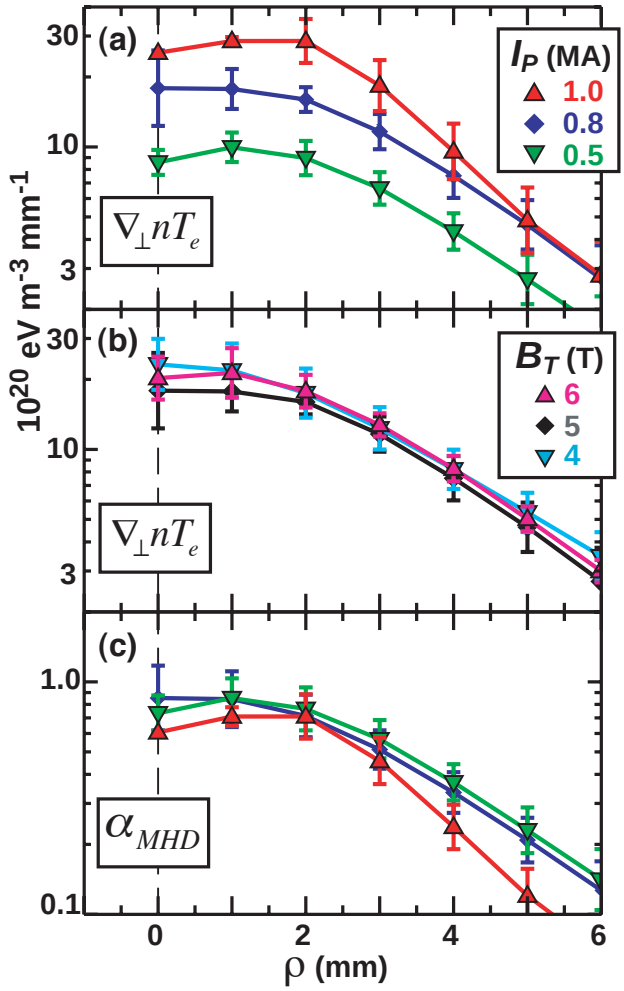

Figure 14. Cross-field profiles of electron pressure gradient [(a) and (b)] and α_{MHD} (c) for a selection of ohmic L-mode discharges in which α_d at the location ρ = 2 mm is approximately the same, $\alpha_d \sim 0.3$. Curves represent average profiles; vertical bars indicate ±1 standard deviation computed from the discharge-to-discharge variation. The absolute pressure gradient is seen to increase with $\sim I_p^2$ [panel (a), data with B_T = 5.3 tesla] such that α_{MHD} maintains a similar value at ρ = 2 mm [panel (c)]. No explicit dependence of the pressure gradient on the value of the toroidal magnetic field [panel (b), data with I_p = 0.8 MA] is detected.

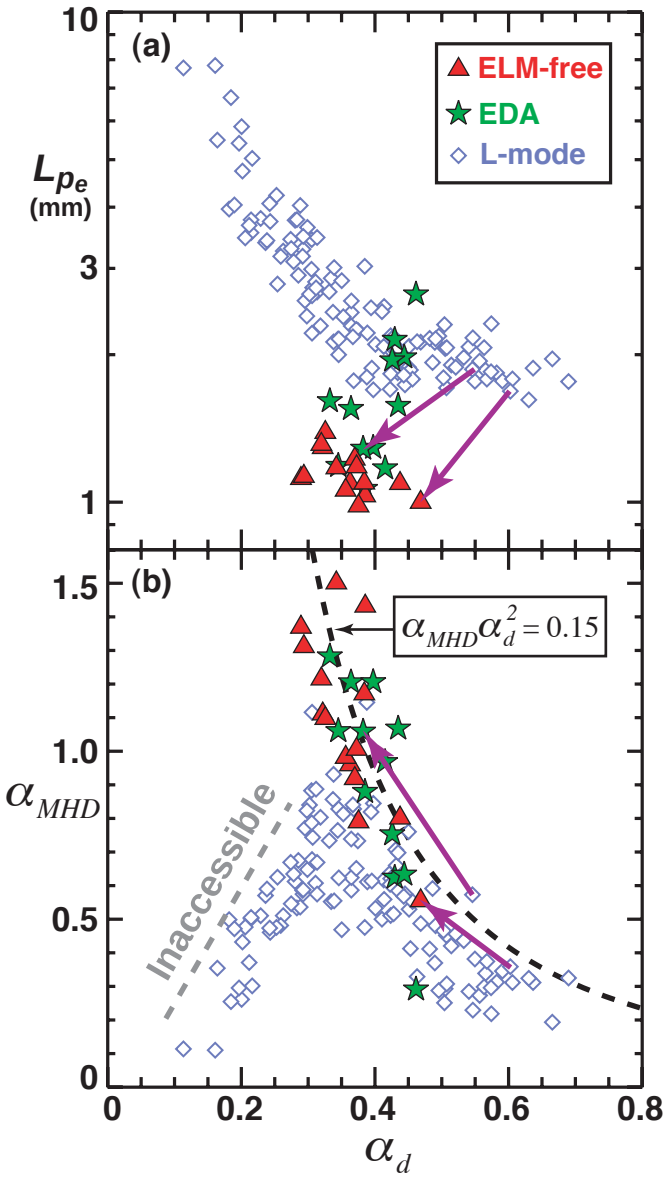

Figure 15. Pressure gradient scale lengths (a) and α_{MHD} (b) at ρ = 2 mm, plotted versus the local value of α_d for the full range of discharges studied (see survey in Fig. 3). Ohmic H-mode data points are indicated by red triangles (ELM-free) and green stars (EDA H-modes). Data obtained during L and H-mode phases of the same discharge are connected by arrows (two cases are shown). The dashed black line indicates the parameterization, $\alpha_{MHD}\alpha_d^2 = 0.15$, which corresponds to a possible L-H threshold condition identified by RDZ [9] and Guzdar [57]. The lack of any stationary L-mode states above and to the right of the dashed line is consistent with the idea that states in this zone are unstable and evolve into H-modes.

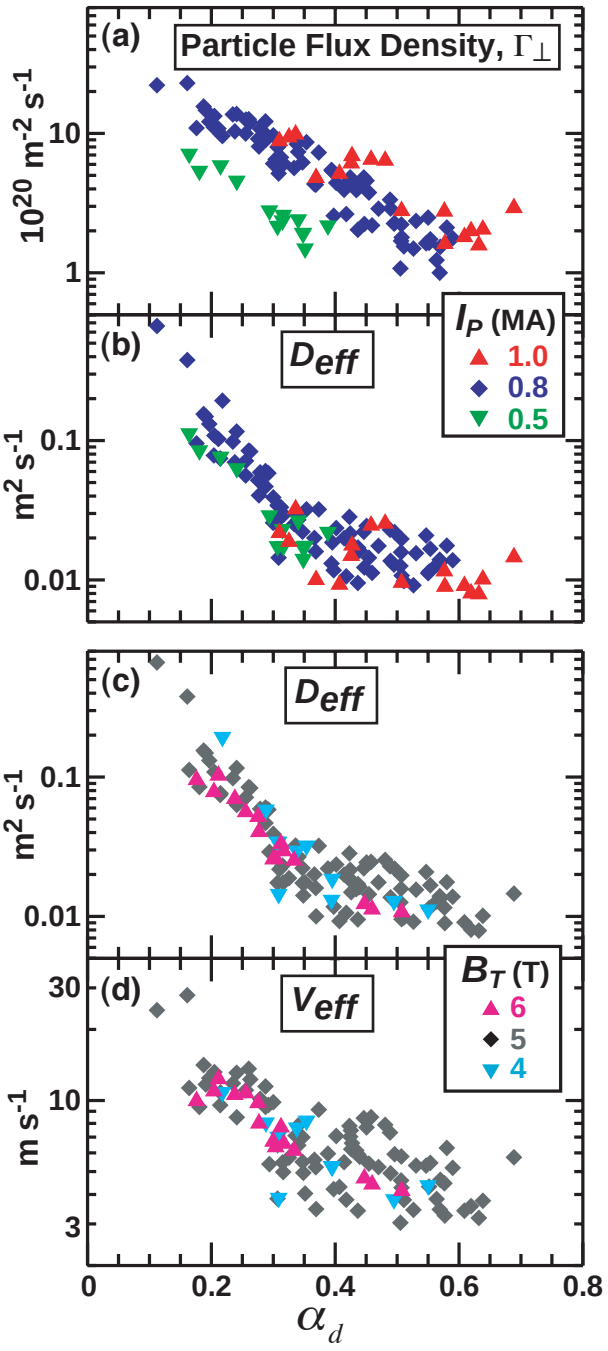

Figure 16. Cross-field particle flux densities at ρ = 2 mm estimated from SOL particle balance (a) and corresponding effective cross-field diffusivities (b, c) and convection velocities (d), plotted versus local values of α_d. Over the range of discharge conditions studied, D_{eff} values are seen to cluster about a monotonic function of α_d, particularly for α_d < 0.35. No explicit dependence of D_{eff} on toroidal magnetic field strength is evident [panel (c)].

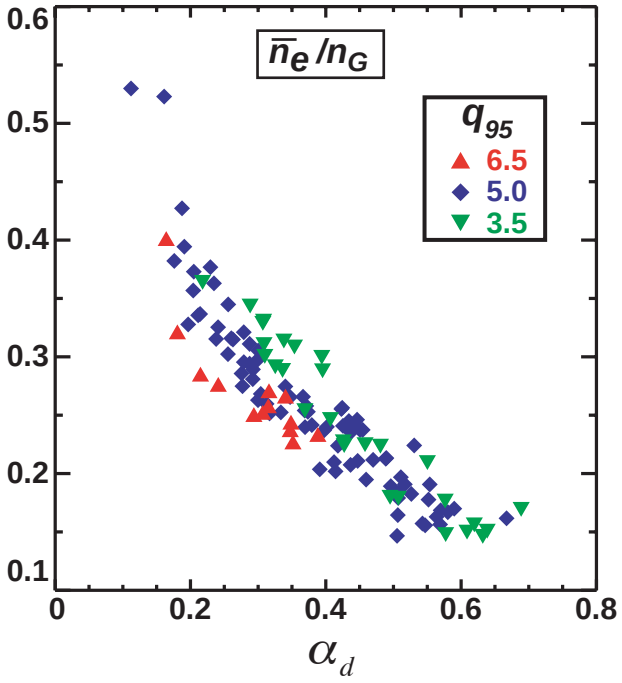

Figure 17. Normalized line-averaged density ($\bar{n}_e/n_G$) versus α_d, evaluated at the location $\rho = 2$ mm. These two quantities are seen to be well correlated (allowing a monotonic function of $\bar{n}_e/n_G$ to be used as a rough proxy for α_d when direct measurement of this quantity is not available). As the discharge density is increased, α_d in the near SOL decreases, resulting in reduced beta gradients (Fig. 15) and larger cross-field fluxes through the SOL (Fig. 16).

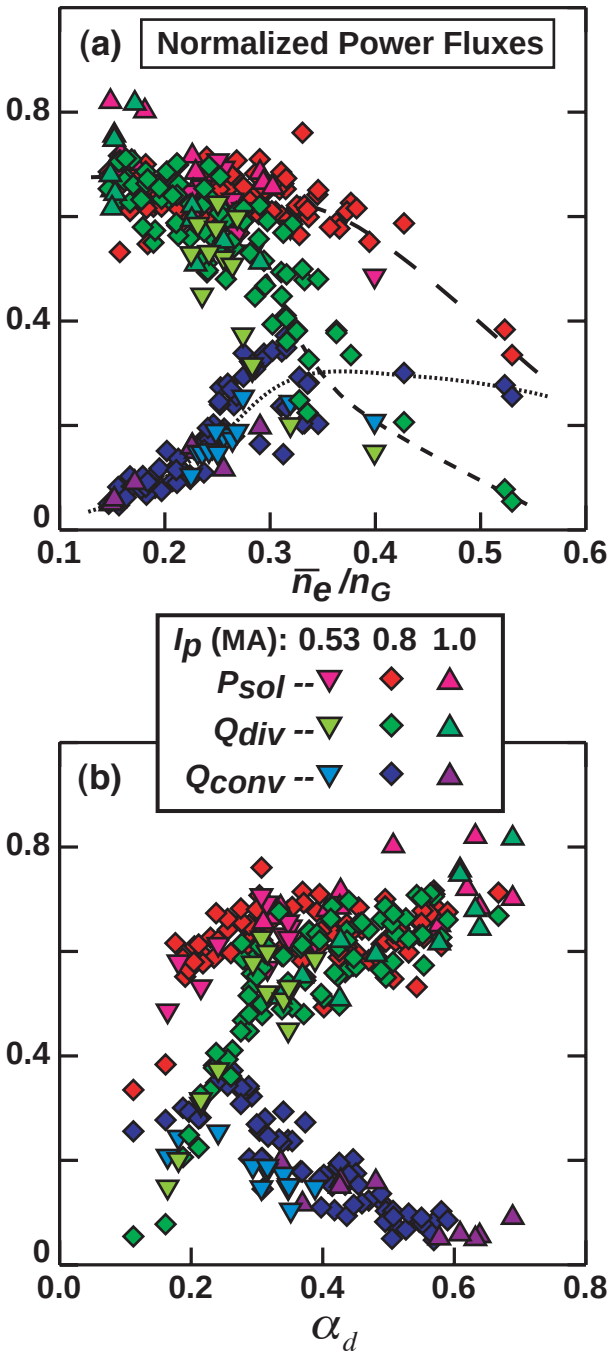

Figure 18. Normalized power fluxes in the SOL, plotted as a function of two different 'control parameters', (a) normalized line-averaged density, $\bar{n}_e / n_G$. and (b) α_d measured at the location ρ = 2 mm. The total input power in the discharge is used to normalize the following quantities: P_{sol} - power flowing into SOL based on input power minus core radiation, Q_{div} - power conducted along field lines to divertor based on $T_e^{7/2}$ integration across SOL, and Q_{conv} - an estimate of power convected across the separatrix based on particle balance. Data points are from the full set of L-mode discharges surveyed in Fig. 3. Below α_d ~0.3, electron parallel conduction to the divertor no longer dominates the power loss in the SOL. Concurrently, the

relative importance of cross-field heat convection systematically increases as α_d decreases. As pointed out in [5, 16], $\bar{n}_e / n_G$ can be used to differentiate between these regimes [panel (a)]. However, based on the close grouping of the green Q_{div} points in panel (b), the relative strength of cross-field to parallel heat transport appears to be more intimately connected to the value α_d near the separatrix.